

# **INTEGRATION OF LOCALIZED SURFACE GEOMETRY IN FULLY PARAMETERIZED ANCF FINITE ELEMENTS**

Gang He<sup>1</sup>  
Mohil Patel<sup>2</sup>  
Ahmed Shabana<sup>2</sup>

<sup>1</sup>College of Mechanical & Electrical Engineering, Hohai University, Changzhou, Jiangsu, 213022, China

<sup>2</sup>Department of Mechanical and Industrial Engineering, University of Illinois at Chicago, 842 West Taylor Street, Chicago, IL 60607-7022

## ABSTRACT

This paper introduces a new method for the integration of localized surface geometry with fully parameterized *absolute nodal coordinate formulation* (ANCF) finite elements. In this investigation, ANCF finite elements are used to create the global geometry and perform the finite element (FE)/multibody system (MBS) analysis of deformable bodies. The localized surface geometry details can be described on ANCF element surfaces without the need for mesh refinement. The localized surface is represented using a standard computational geometry method, Non-uniform rational B-spline surface (NURBS), which can describe both conic surface and freeform surface efficiently and accurately. The basic idea of the integration of localized surface geometry with ANCF elements lies in the inclusion of such detail in the element mass matrix and forces. The integration can be implemented by overlapping the localized surface geometry on the original ANCF element or by directly trimming the ANCF element domain to fit the required shape. During the integration process, a mapping between ANCF local coordinates and NURBS localized geometric parameters is used for a consistent implementation of the overlapping and trimming methods. Additionally, two numerical integration methods are compared for the rate of convergence. The results show that the proposed subdomain integration method is better, since it is optimized for dealing with complex geometry. The proposed subdomain method can be used with any fully parameterized ANCF element. In order to analyze the accuracy of the proposed method, a cantilever plate example with localized surface geometry is used, and the simulation results with the proposed method are compared with the simulation results obtained using a commercial FE code. Two other examples that include contact with ground and localized surface geometry are also provided. These examples are a simple plate structure with surface geometry and a tire with tread details. The incompressible hyperelastic Mooney-Rivlin material model is used to describe the material used in the tire tread. It is shown through the tire contact patch that the proposed method can successfully capture the effect of the tread grooves. The rate of convergence and locking of fully parameterized ANCF elements are also discussed in this paper.

**Keywords:** Localized surface geometry; absolute nodal coordinate formulation; subdomain integration; multibody system dynamics; contact; tire tread; Mooney-Rivlin; NURBS.

## 1. INTRODUCTION

Because detailed localized surface geometry is found in many structural and mechanical system applications, considering the effect of such geometry during the FE or flexible MBS analysis is important. An example of localized geometry that affects the behavior of a system is the tread details in a tire. Table 1 shows a classification of the different kinds of tread details that are specific to the application type of the tire they are designed for. In some cases, simplification of the tire model by ignoring such details may be a reasonable assumption, however in certain analyses like hydroplaning situations ignoring the tread details can lead to incorrect results. Hence, including localized geometry in the FE or flexible MBS analysis is essential in certain simulation scenarios.

When classical FE methods are used with MBS dynamics codes, difficulties are encountered in achieving the correct solution for problems involving large deformation and rotation due to the incremental-rotation assumptions used in existing FE formulations (Neto et. al, 2004; Shabana, 1997; Das et. al, 2010). The ANCF method which uses absolute positions and gradients as nodal coordinates can not only capture correct rigid body motion and large deformation but also has the advantages of a constant inertia matrix and zero Coriolis and centrifugal forces (Orzechowski and Fraczek, 2012; Orzechowski and Fraczek, 2015; Tian et al., 2014; Shabana 2012; Shabana and Yakoub, 2001; Recuero et. al, 2014), and can describe a freeform surface's geometry accurately (Sanborn and Shabana, 2009; Lan and Shabana, 2010). Due to the fact that a non-incremental solution procedure can be used, ANCF elements can be easily implemented in general purpose MBS algorithms (Shabana, 2014; Shabana, 2015; Shabana, 2013; Patel et. al, 2015). Although ANCF has many advantages in the simulation of very flexible bodies as demonstrated by the already published investigations, the representation

of localized surface geometry, such as holes, grooves and protrusions which can play significant roles in the overall dynamics of the structure, without mesh refinement remains a challenge (Cho et. al, 2004; Gipser, 2005; Lugner et. al, 2005; Pacejka, 2006). Depending on the goal of the simulation, ignoring such details could potentially lead to incorrect solutions (Cho et. al, 2004).

Capturing detailed localized geometry is a challenging research topic in the Computer Aided Design (CAD) field as well (Li and Ke, 2000; Schmidt, 2012). In the CAD field, the main methods for representing complex shapes include trimming, sewing and Boolean operations, wherein small surface patches or small solids are used to represent complex geometric shapes; an approach that can be computationally quite expensive and may cause problems such as geometric error or numerical instabilities (Li and Ke, 2000). In order to circumvent such processes in the Computer Aided Engineering (CAE) field, the FE models are often simplified by simply removing local geometric features from the overall body before meshing or subjected to mesh refinement until the desired geometry details are captured (Cho et. al, 2004; Ito, et. al, 2009; Kagan et. al, 2003). Nonetheless as previously mentioned, ignoring some of these geometric details may not be allowable in certain analysis scenarios. On the other hand refining the mesh may cause the mesh data to increase exponentially and prolong the computation time greatly. Sometimes a very fine mesh can make the analysis almost impossible because of the limitations on the computer memory and processing capabilities. Several researchers have recently focused their investigations on new meshing methods or elements that enable local refinement (Kagan et. al, 2003; Kleiss et. al, 2012) by making use of hierarchical B-splines and NURBS (Bornemann, 2013), T-splines (Uhm and Youn, 2009) and PHT splines (Wang et. al, 2011). Such methods are effective both in reducing the mesh size and obtaining accurate results (Cho, 2004). These methods however are complicated to implement and their effectiveness

depends on the given geometry being analyzed. Furthermore, such methods that are dependent on a rigid recurrence scheme could pose several problems when used with ANCF elements (Sanborn and Shabana, 2009; Gantoi, et. al, 2013).

This paper proposes a new method for the implementation of localized geometry into ANCF surfaces. The proposed method can be used with any fully parameterized ANCF element. This paper is organized as follows: Section 2 reviews the three levels of including localized surface geometry in FE methods. Section 3 briefly introduces the concepts and methodologies used in the definition of fully parameterized ANCF elements. Section 4 describes two methods of integrating localized surface geometry with ANCF elements. Section 5 compares the results obtained using the global domain integration method and subdomain integration method. Section 6 briefly describes the governing equations of motion and the contact method used in the numerical examples presented in this paper. Section 7 presents three examples and compares the results obtained using the approach described in this paper with the results obtained using a commercial FE code in order to demonstrate the effectiveness of the proposed approach.

## **2. LOCALIZED SURFACE GEOMETRY MODELING METHODS**

There are three different levels in the FE analysis at which the local surface geometry can be implemented in the model. For level one, the geometry details are included while building the CAD model, for level two, these details are included while generating the FE mesh, and for level three, the details are included during the numerical integration process of the FE problem. Thus the localized surface geometry modeling approach can be classified as the geometric shape design level (Kagan, et. al, 2003; Bouclier, 2016; Chemin et. al, 2015), mesh level and numerical integration level (Wang, 2000; Nicolas and Fouquet, 2013).

In the CAD field, the techniques used to represent the localized geometry mainly include local and global refinement methods, trimming and the merging methods (Piegl and Tiller, 1997; Schmidt et. al, 2012). Global refinement is the simplest refinement technique in geometric design (Li and Ke, 2000). For example, the most useful method when B-spline and NURBS are used is to insert knots where the local feature exists (Kagan et. al, 2003; Yu et. al, 2016). However, the patches near the local geometric feature must be refined simultaneously to ensure conformity, and this may introduce many undesired control points. The disadvantage of this approach is that it leads to rapidly growing computing and storage requirements. Trimmed NURBS surface has become one of the most effective and widely used methods in current CAD systems for modeling complex surfaces because it provides a promising alternative for representing NURBS domains of arbitrarily complex topology (Schmidt et al, 2012). The trimmed NURBS surface approach makes adding localized surface geometry convenient and easy. One disadvantage of the trimmed NURBS surface method is that it can lead to difficulties during mesh generation, by often making the mesh irregular and overly fine, which may lead to highly deformed elements in the reference configuration, error in the FE solution due to a distorted mesh, and a higher computational cost in case of an overly fine mesh. In order to improve the flexibility of splines and enable local refinement, several new splines have been developed recently, including hierarchical B-splines and NURBS (Bornemann et. al, 2013, Bouclier et. al, 2016), LRB-splines and T-splines (Uhm and Youn, 2009; Wang et. al, 2011; Schillinger et. al, 2012). T-splines have attracted considerable attention in both the computational geometry and analysis communities since they can also represent trimmed multi-patch geometries. PHT-splines which are based on T-splines have been used in the framework of isogeometric analysis (Bouclier et. al, 2016). Forsey and Bartels (1998) introduced the concepts of hierarchical B-splines, which provide the

capability for local refinement of surfaces and multi-resolution surface editing. Since this method is not restricted to the underlying B-spline mathematics, it is applicable to any parametric tensor product or triangular representation. There are several methods in the CAD field for localized surface geometry modeling, but it is difficult to use them in conjunction with ANCF since they are very complicated to implement and might lead to issues regarding the continuity and conformity between elements which is an important aspect of the ANCF method.

Methods for the inclusion of localized geometry at the mesh level also consist of global refinement and local refinement. There are several major approaches that allow adaptive refinement in the FE analyses including the h-refinement, p-refinement and r-refinement (Chemin et. al, 2015; Wang, 2000). H-refinement is considered a non-local refinement method because more than one element is refined at the same time. The algorithm for h-refinement is simple and it is easy to apply to complicated domains. There are similar refinement techniques based on a hierarchical split of the standard finite element which allow localized surface geometry modeling (Wang, 2000; Nicolas 2013). However, most adaptive mesh refinement methods are approximations of the original mesh to within a given tolerance, and therefore, conformance of the elements can be difficult to achieve. Furthermore, as finer meshes are being developed in order to capture fine geometry details, the computing and storage requirements and the number of degrees of freedom of the mesh increase. Since the ANCF method employs higher order displacement polynomials in order to achieve gradient continuity, conformance in some elements, and more detailed deformation shapes, ANCF elements normally have more degrees of freedom as compared to the classical FE's which can lead to long simulation time.

In the FE method, the inertia and elastic force coefficients in the weak form of the equilibrium equations are evaluated using numerical integration methods. Hence the influence of

a local geometric shape can also be considered by adjusting the integration domain or the distribution of integration points when calculating these inertia and force coefficients which are required in order to obtain the solution of the FE problem. The detailed localized surface can be described by a curve or surface which is then used to adjust the integration points. In this case, the original mesh does not need to be refined to the size factor of the geometric feature to be captured. Integration point level methods include the subdomain method and the adaptive integration method. In the adaptive integration method, the mesh or the geometric domain area can be divided into several smaller domains that use different integration methods depending on the accuracy requirements or shape representation (Bouclier et. al, 2016; Schillinger et. al, 2012). Recently, a large number of investigations have been focused on virtual domains and meshless methods which can be considered as numerical methods developed for inclusion of details and features that cannot be easily captured using the traditional FE shape functions (Schillinger et. al, 2012). When ANCF elements are used, it is more practical to use the integration point level method to model localized surface geometry because this method does not require any kind of mesh refinement and it is easy to implement.

### **3. ANCF GEOMETRY**

In MBS applications, the method used to create the model geometry as well as to analyze the FE mesh developed using this geometry must ensure the consistency and accuracy of the results. ANCF has shown its versatility in dealing with complex geometry such as tires, leaf springs, tank cars etc. (Patel, et. al, 2015; Yu et. al, 2016). This section briefly reviews the ANCF equations that will be used in other sections of this paper.



Flexible bodies that undergo large deformation do not always have uniform dimensions throughout the body. For example, the geometric shape and transverse deformation in the thickness cannot always be ignored. Considering this modeling complexity, fully parameterized ANCF elements are good choices for the analysis of large deformation problems. Amongst the collection of fully parameterized ANCF elements, the conforming plate element, which ensures gradient continuity on the element edges, is selected for the development presented in this investigation (Mikkola and Shabana, 2003). The global position vector of an arbitrary point on an ANCF plate element  $j$  on body  $i$  can be defined using the element generalized coordinates  $\mathbf{e}^{ij}$  and the element shape function matrix  $\mathbf{S}^{ij}$  as  $\mathbf{r}^{ij}(x, y, z) = \mathbf{S}^{ij}(x, y, z)\mathbf{e}^{ij}(t)$ , where  $t$  is time, and  $(x, y, z)$  are the element local coordinates. The vector of nodal coordinates  $\mathbf{e}^{ij}$  can be written as  $\mathbf{e}^{ij}(t) = [\mathbf{e}_1^{ijT} \quad \mathbf{e}_2^{ijT} \quad \mathbf{e}_3^{ijT} \quad \mathbf{e}_4^{ijT}]^T$ , where the subscript refers to the node number. The generalized coordinates at a given node  $k$  include absolute position and three gradient vector coordinates, which can be written as  $\mathbf{e}_k^{ij} = [(\mathbf{r}_k^{ij})^T \quad (\partial \mathbf{r}_k^{ij} / \partial x)^T \quad (\partial \mathbf{r}_k^{ij} / \partial y)^T \quad (\partial \mathbf{r}_k^{ij} / \partial z)^T]^T$  for  $k = 1, 2, 3, 4$ . When fully parameterized ANCF elements are used to represent the flexible bodies, the parameter  $z$  can be expressed as a function of  $x$  and  $y$ , allowing the thickness of the element to vary with the other two local coordinates. Using this concept, the position vector of an arbitrary point on the element can be defined as  $\mathbf{r}^{ij}(x, y, z) = \mathbf{S}^{ij}(x, y, f(x, y))\mathbf{e}^{ij}(t)$ , this equation is obtained by simply substituting the local coordinate  $z$  using a function  $f(x, y)$  (Gantoi et. al, 2013). Using this simple method, any given localized surface geometry can be described in the ANCF element without the need for further mesh refinement. By writing one parameter,  $z$ , in terms of the other two parameters,  $x$  and  $y$ , a surface with an arbitrary shape can be defined

using the function relationship  $z = f(x, y)$ . The function  $f(x, y)$  can be used to represent complex geometry and can also be defined analytically or numerically.

#### 4. INTEGRATION OF LOCALIZED SURFACE

This section introduces the integration of localized surface geometry with the global ANCF surface geometry. The concept of NURBS which is used to describe localized surface geometry is also briefly introduced.

##### 4.1 The Definition of Localized Surface

In this investigation, the localized surface geometry to be integrated with the fully parameterized ANCF elements is defined using the NURBS representation, which is a generalized version of the B-spline method and has become a standard geometric modeling method in CAD and computer graphics industries. Unlike general Lagrange polynomials, NURBS can describe a circle and sphere exactly and will be briefly reviewed in this section. Let  $\mathbf{U} = (u_1, u_2, \dots, u_{n+p+1})$ , called the knot vector, be a non-decreasing sequence of parameter values, where  $p$  is the degree of the NURBS curve,  $n$  is the number of control points, and  $u_i$  is the knot value and the set of all knot values makes up the knot vector  $\mathbf{U}$ . The  $i$ -th B-spline basis function of degree  $p$ , denoted by  $N_{i,p}(u)$  is defined as (Piegl and Tiller, 1997)

$$\left. \begin{aligned} N_{i,0}(u) &= \begin{cases} 1 & u_i < u < u_{i+1} \\ 0 & \text{otherwise} \end{cases} \\ N_{i,p}(u) &= \frac{u - u_i}{u_{i+p} - u_i} N_{i,p-1}(u) + \frac{u_{i+p+1} - u}{u_{i+p+1} - u_{i+1}} N_{i+1,p-1}(u) \end{aligned} \right\} \quad (1)$$

B-spline curves are defined as follows:

$$\mathbf{c}(u) = \sum_{i=0}^n N_{i,p}(u) \mathbf{P}_i \quad (2)$$

where  $\mathbf{P}$  is the vector of control points of the B-spline curve. NURBS curve, which is the weighted and rational form of B-spline, can be expressed as follows (Piegl and Tiller, 1997):

$$\mathbf{c}(u) = \frac{\sum_{i=0}^n N_{i,p}(u) w_i \mathbf{P}_i}{\sum_{i=0}^n N_{i,p}(u) w_i} \quad (3)$$

where  $w_i$  is the weight of  $i$ -th control point. A NURBS surface of degree  $p$  in the direction  $u$  and degree  $q$  in direction  $v$  is represented as follows (Piegl and Tiller, 1997):

$$\mathbf{p}(u, v) = \frac{\sum_{i=0}^n \sum_{j=0}^m N_{i,p}(u) N_{j,q}(v) w_{ij} \mathbf{P}_{ij}}{\sum_{i=0}^n \sum_{j=0}^m N_{i,p}(u) N_{j,q}(v) w_{ij}} \quad (4)$$

where the size of control points matrix  $\mathbf{P}_{ij}$  and weights  $w_{ij}$  is  $n \times m$ .

## 4.2 Localized Geometry and ANCF Elements

In this section, two methods for integrating the localized geometry with ANCF elements are described. The global geometry of the structure is represented by the ANCF shape functions and the element nodal coordinates, whereas the shape of localized geometry is described using the NURBS representation. As mentioned earlier the basic ANCF geometry that the localized geometry is superimposed on can be defined as  $\bar{\mathbf{r}}(x, y, z) = \mathbf{S}(x, y, z) \mathbf{e}(t)$ . In this section,  $\mathbf{r}$  refers to the ANCF element geometry that accounts for the local geometry features, whereas  $\bar{\mathbf{r}}$  refers to the ANCF geometry without localized geometry modifications. When a local feature such as a protrusion is added in an element domain  $\Omega_l$ , its shape can be defined by overlapping a height

value on the basic element shape along a direction normal to the surface. Accordingly, the modified position field with the groove in the element can be denoted as

$$\mathbf{r}(x, y, z) = \begin{cases} \bar{\mathbf{r}}(x, y, z) & (x, y) \notin \Omega_l \\ \bar{\mathbf{r}}(x, y, z) + h(x, y)\mathbf{n} & (x, y) \in \Omega_l \end{cases} \quad (5)$$

where  $\mathbf{n}$  is the normal to the basic ANCF mid-surface calculated as  $\mathbf{n} = (\bar{\mathbf{r}}_x \times \bar{\mathbf{r}}_y) / |\bar{\mathbf{r}}_x \times \bar{\mathbf{r}}_y|$ ,  $h(x, y)$  is the thickness of the localized geometry, which may be represented by a NURBS curve or surface, and  $\Omega_l$  is the domain on which localized geometry is defined. As shown in Fig. 1(a), if the height is set to a positive value, a protrusion can be defined in the ANCF element. This method can also be used to define other localized geometries by defining different NURBS curves and surfaces.

Another method that is quite useful in defining localized surface geometry, especially when dealing with features like a groove, can be implemented by trimming a given ANCF domain with a boundary curve described by NURBS as is illustrated in Fig. 1(b). This method can be more general than the overlapping method particularly when multiple curves or surfaces are used to define the boundary. However, for the fully parameterized ANCF elements considered in this investigation, we mainly focus on the simple situation of a single type of localized geometry, so only one NURBS curve or NURBS surface is used to define the trimming boundary. The easiest way to implement this method is to augment the original thickness domain of the element from  $z_0 \in [-0.5, 0.5]$  to either  $z \in [z_{min}, 0.5]$  or  $z \in [-0.5, z_{max}]$  where the upper and lower surface of the element can be locally defined by the dimensionless coordinates  $z_{max}$  and  $z_{min}$  respectively which may be controlled by a function  $f(x, y)$ , and  $[\cdot]$  refers to a closed interval.

Since during the numerical integration process  $(x, y, z)$  are the local coordinates in the element straight configuration and the parameters of NURBS are commonly based on the arc length of the curve or the isoparametric curves, a mapping,  $(x, y) \rightarrow (u, v)$ , is required between the ANCF local coordinates and NURBS localized geometric parameters, which is shown in Fig. 2. For example, if the localized geometry is defined on the top surface of the ANCF element, the domain of this geometry can be defined along the element longitudinal and lateral directions as  $x \in [0, 1]$  and  $y \in [y_a, y_b]$  respectively. However the range of the function defining the geometry may only vary with  $y$ . For such geometry and for the overlapping and the trimming methods described in this section, the mapping process between ANCF and NURBS can be summarized as follows:

- Step 1: If  $y \in [y_a, y_b]$ ,  $\bar{y} = (y - y_a) / (y_b - y_a)$ , go to Step 2; otherwise go to Step 5.2
- Step 2: Initialize  $u_0 = \bar{y}$
- Step 3: Carry out Newton iteration:  $\bar{u}_{k+1} = \bar{u}_k - \mathbf{B}^T \mathbf{c}'(\bar{u}_k) / \mathbf{B}^T \mathbf{c}''(\bar{u}_k)$ , where  $\mathbf{B} = [0 \ 1 \ 0]^T$
- Step 4: If  $|\bar{u}_{k+1} - \bar{u}_k| > \varepsilon$ , where  $\varepsilon$  is a specified tolerance, go to Step 3, otherwise go to step 5.1
- Step 5.1:  $(x, y, z_{\max}) = \mathbf{c}(\bar{u}_{k+1})$
- Step 5.2:  $(x, y, z_{\max}) = (x, y, 0.5)$
- Step 6: Calculate numerical integration points and weights in vertical domain  $[-0.5, z_{\max}]$
- Step 7: Calculate actual element global coordinates by either overlapping or domain trimming method

Using the procedure described in this section, the mapping between the NURBS parameters and the ANCF local coordinates can be achieved, and the localized geometry can be superimposed on the ANCF surface.

## 5. NUMERICAL INTEGRATION METHOD

The basic idea of the FE method is to approximate the governing differential equations of the flexible body by mesh discretization and numerical integration. Mesh refinement is currently the only way to define detailed geometry using ANCF elements. A very fine mesh of ANCF elements without parallel computation could lead to long simulation run times. Since the computational implementation of the finite element method as well as the new concepts proposed in this paper heavily rely on numerical integration, this section will discuss the numerical integration method used and its accuracy.

### 5.1 Global Domain and Subdomain Integration Method

The number and distribution of the integration points has a significant influence on the simulation accuracy. The Gauss integration method is the standard method used in the FE analysis since it is the most accurate numerical integration method for a given number of integration points. Therefore, the Gauss integration method is used in this investigation as well. In order to integrate the localized geometry in this investigation, two methods: the global domain and the subdomain methods are used and compared.

In the global domain integration method, there is only one integration domain  $\Omega_g$  for every element, and an integration point can be identified by its coordinates in the element as  $\mathbf{q}_i = (x_i, y_i, z_i) = (x_i, y_i, f(x_i, y_i))$ . A function  $\varphi(x_i, y_i, z_i)$  can be numerically integrated using the global domain method as

$$\Gamma_g = \sum_{i=1}^{n_g} \varphi(x_i, y_i, z_i) w_i = \sum_{i=1}^{n_g} \varphi(x_i, y_i, f(x_i, y_i)) w_i \quad (7)$$

where  $n_g$  is the total number of integration points, and  $w_i$  is the weight corresponding to that integration point. The weights are usually dependent on the orthonormal functions used in the integration scheme.

In the subdomain integration method, on the other hand, the whole domain  $\Omega$  of an element is divided into  $n_d$  subdomains  $\Omega_1, \Omega_2, \dots, \Omega_{n_d}$  where this set of subdomains satisfies  $\Omega = \Omega_1 \cup \Omega_2 \cup \dots \cup \Omega_{n_d}$  and  $\Omega_k \cap \Omega_l = \emptyset$  when  $k \neq l$ . There are  $\bar{n}_i$  integration points in each subdomain  $\Omega_j$ , and the function  $\varphi(x_i, y_i, z_i)$  can be numerically integrated on  $\Omega$  using the subdomain method as

$$\Gamma_l = \sum_{j=1}^{n_d} \sum_{i=1}^{\bar{n}_i} \varphi(\bar{x}_{ji}, \bar{y}_{ji}, f(\bar{x}_{ji}, \bar{y}_{ji})) \bar{w}_{ji} \quad (8)$$

where  $\bar{w}_{ji}$  is the integration weight related to the corresponding integration point defined by  $\bar{\mathbf{q}}_{ji}$ .

Figure 3 shows the distribution of integration points generated by the two integration methods in the same integration domain that includes localized geometry. One major difference between the two methods is that the subdomain method allows for much more flexibility and control of integration points in the domain that is being integrated since the regular single domain or global domain integration is constrained by the abscissa of the integration points which are the roots of the Legendre polynomial, whereas with the subdomain integration the subdomains can be adjusted based on the configuration of the local geometry. As can be seen in Fig. 3, the global domain integration method leads to 3 integration points capturing the localized geometry, whereas the use of the subdomain method would lead to 9 integration points capturing the effect of the localized geometry and leading to more accurate results.

## 5.2 Comparison of the Two Integration Methods

Figure 4 compares the two integration methods described previously in this section. Figure 4(a) shows the discretization of the element in the  $y$  direction using the subdomain method. The element thickness is varied using the function  $z = f(y)$  defined on the domain  $[y_1, y_6]$ , wherein the local geometry feature of interest is located in the middle of the given domain. The whole domain is divided into five subdomains, of which subdomains  $[y_2, y_3]$ ,  $[y_3, y_4]$  and  $[y_4, y_5]$  are used to define the local feature. Figure 4(b) shows the detailed localized geometry shape, which is represented by a NURBS curve and its control points, which are also shown in the figure. In order to compare between the global and subdomain integration methods, the norm of the mass matrix is evaluated for a plate element with the localized geometry given in Fig. 4(a) and 4(b) superimposed on its lower surface. Figure 4(c) shows the results of the norm of the mass matrix evaluated using the two numerical integration methods. The mass matrix of ANCF elements is

defined as  $\mathbf{M} = \int_V \rho \mathbf{S}^T \mathbf{S} J_o dV$ , where  $\rho$  is the mass density,  $V$  is the volume in the straight

configuration, and  $J_o$  is the determinant of the matrix of position vector gradients that define the curved geometry in the reference configuration. In this example, the density  $\rho$  is assumed to be  $1500 \text{ kg/m}^3$ , the length and width both are taken to be  $1 \text{ m}$ , and the thickness is  $0.05 \text{ m}$ . As can be seen in Fig. 4(c), while using the subdomain integration method, increasing the number of integration points to more than 3 in every subdomain leads to faster convergence in the norm of the mass matrix. However when using the global domain integration method, even increasing the number of integration points to more than 40 does not lead to satisfactory convergence of the norm of the mass matrix. These results show that local and more dense distribution of the



integration point mesh using the subdomain method is a better choice considering the balance between solution accuracy and computational cost.

## 6. ANCF GOVERNING EQUATIONS

In this investigation, the dynamic equations of motion are formulated using ANCF elements. This formulation leads to a constant mass matrix and nonlinear elastic force vector. Regardless of the complexity of the geometry superimposed on the ANCF elements, the mass matrix remains constant and the Coriolis and centrifugal forces are identically zero vectors. Using the expressions of the kinetic energy, strain energy and the virtual work of external forces, the dynamic equations of the ANCF element can be defined in the form  $\mathbf{M}\ddot{\mathbf{e}} + \mathbf{Q}_k = \mathbf{Q}_e$ , where  $\mathbf{M}$  is the mass matrix,  $\mathbf{e}$  is the vector of nodal coordinates,  $\mathbf{Q}_k$  is the vector of elastic forces, and  $\mathbf{Q}_e$  is the vector of generalized external forces including the gravity force and contact force  $\mathbf{Q}_c$ . Using the continuum mechanics approach, the virtual work of the elastic forces of fully parameterized elements can be written as  $\delta W_k = - \int_V \boldsymbol{\sigma}_{p2} : \delta \boldsymbol{\varepsilon} dV$  where  $\boldsymbol{\sigma}_{p2}$  is the second Piola-Kirchhoff stress tensor conjugate to  $\boldsymbol{\varepsilon}$  which is the Green-Lagrange strain tensor defined as  $\boldsymbol{\varepsilon} = \frac{1}{2}(\mathbf{J}^T \mathbf{J} - \mathbf{I})$ , where  $\mathbf{J}$  is the matrix of position vector gradients. In case of a curved reference configuration  $\mathbf{J} = \frac{\partial \mathbf{r}}{\partial \mathbf{X}} = \left( \frac{\partial \mathbf{r}}{\partial \mathbf{x}} \right) \left( \frac{\partial \mathbf{x}}{\partial \mathbf{X}} \right) = \mathbf{J}_e \mathbf{J}_o^{-1}$  where  $\mathbf{r}$  and  $\mathbf{X}$  are, respectively, the position vector of a material point in the current configuration and reference configuration, and  $\mathbf{x} = [x \ y \ z]^T$  is the vector of element spatial coordinates. For generality,  $\boldsymbol{\sigma}_{p2}$  can be derived from the strain energy function as  $\boldsymbol{\sigma}_{p2} = 2\partial U / \partial \mathbf{C}_r$ , where  $U$  is the strain energy potential

function, and  $\mathbf{C}_r$  is the right Cauchy-Green deformation tensor defined as  $\mathbf{C}_r = \mathbf{J}^T \mathbf{J}$  (Ogden, 1984; Shabana, 2012). In the case of the hyperelastic nearly incompressible Mooney-Rivlin material model used in one of the examples in this investigation,  $U = \mu_{10}(\bar{I}_1 - 3) + \mu_{01}(\bar{I}_2 - 3) + \frac{1}{2}k(J - 1)^2$  where  $\mu_{10}$ ,  $\mu_{01}$  are material coefficients,  $\bar{I}_1$ ,  $\bar{I}_2$  are the invariants of the deviatoric part of the  $\mathbf{C}_r$  tensor,  $k$  is the penalty term and  $J = |\mathbf{J}|$  (Ogden, 1984; Shabana, 2012; Orzechowski and Fraczek, 2015).

A simple contact model based on a penalty approach and coulomb friction is used in this investigation. The contact forces are treated as point forces where the normal component is defined as  $\mathbf{f}_n = (k_p d + c_p \dot{d})\mathbf{n}$ , where  $\mathbf{f}_n$  is the normal component of the contact force,  $k_p$  is the ground stiffness coefficient,  $c_p$  is the ground damping coefficient,  $d$  and  $\dot{d}$  are the penetration and the rate of penetration respectively, and  $\mathbf{n}$  is the unit normal to the ground surface at the contact point. The penetration is calculated as  $d = (\mathbf{r}_p - \mathbf{r}_p^g) \cdot \mathbf{n}$ , where  $\mathbf{r}_p$  is the global position of the contact point on the flexible body, and  $\mathbf{r}_p^g$  is the global position of the corresponding contact point on the ground (Patel, et. al, 2015; Gantoi et. al, 2013). For the tangential contact forces, each contact point is detected for its relative velocity with respect to the ground in order to apply the tangential force that depends on the coefficient of friction  $\mu$ . The expression for the generalized contact forces associated with the ANCF generalized nodal coordinates can be obtained by using the virtual work of the contact forces and is given by  $\mathbf{Q}_c = \mathbf{S}(\mathbf{x})^T \mathbf{f}_c$ , where  $\mathbf{f}_c = \mathbf{f}_n + \mathbf{f}_t$ , where subscripts  $n$  and  $t$  refer to normal and tangential directions, respectively.

## 7. NUMERICAL RESULTS

Three numerical examples are presented in this section to demonstrate the method of adding localized surface geometry. In the first example, a plate-like structure with localized geometry meshed with ANCF plate elements is used in the simulation of contact with a ground. Different numbers of subdomains and integration points are used to compare their influence on the accuracy of the results. In the second example, the deformation of a cantilever plate with grooves under a concentrated force at a corner of the free end is simulated and the results are compared with the results obtained using a commercial FE code (ANSYS, 2013). In the third example, ANCF plate elements with a nearly incompressible Mooney-Rivlin rubber material are used to model a tire with tread details, and the convergence of this model is demonstrated by refining the tire mesh.

### **7.1 Plate Contact Example**

In this example, localized surface geometry is overlapped on the ANCF elements and the structure is allowed to free fall and contact with a ground. The length and width of the plate element are both 1m and the thickness is 0.05m. The localized geometry that is defined between  $[0.4, 0.6]$  of the non-dimensional  $y$  coordinate of the element is shown in Fig. 5(a). The material and contact properties are given in Table 2 and 3, respectively. There is one integration domain in the vertical and longitudinal directions of the element with 3 and 7 integration points, respectively, whereas the integration domain in lateral direction is divided into several subdomains according to the shape of the localized geometry, and the number of integration points in the lateral subdomains is varied from 2 to 5 in order to examine the effectiveness of the subdomain integration scheme. Figure 5(b) shows the contact patch of one ANCF plate element with localized surface geometry.

In order to analyze the effect of the subdomain division and number of integration points per subdomain, the vertical position of the center point at the plate lower surface is shown. First the influence of the number of integration points per subdomain is analyzed by dividing the element lateral domain into 3 subdomains. As shown in Fig. 6, as the number of integration points per subdomain is increased from 2 to 5, the solution converges. However, it can be seen from the enlarged drawing in Fig. 6 that 3 integration points per subdomain are sufficient for obtaining a converged solution when compared against the computation time taken by 5 integration points per subdomain. The effect of the number of subdomains per element is investigated using the same example. It can be seen from Fig. 7 that increasing the number of subdomains from 2 to 4, with 3 integration points per subdomain yields converged results as well. Furthermore, it can be seen from the enlarged plot in Fig. 7 that 3 subdomains lead to sufficiently converged results. The number of integration points per subdomain and the number of subdomains per element may have to differ for more complicated geometry; however this example shows that the subdomain method is a viable and relatively computationally efficient method for including localized geometry details in an ANCF mesh without further mesh discretization.

Figures 8(a), (b) and (c) show the results of the aforementioned contact example with a  $2 \times 2$  mesh of ANCF plate elements with two grooves representing the localized surface geometry. The localized geometry shape, overall structure dimensions and the material properties are the same as one element mesh. Figure 8(a) shows the time evolution of the vertical position of the center point at the plate lower surface. Figures 8(b) and 8(c) show the contact force distribution at  $t = 1s$ , which clearly shows the effect of the grooves is captured in the contact force distribution.

## 7.2 Cantilever Plate Validation

In order to show that the method proposed in this investigation is able to capture the effect of the local surface geometry, a validation example in the form of a cantilever plate with a tip force at its free end is provided. The ANCF results are compared with those obtained from a commercial FE code (ANSYS, 2013). The conforming fully parameterized plate element is used for the ANCF mesh whereas SOLID186 element which has a quadratic displacement field is used in the commercial FE code. Figure 9 shows the reference configuration of the cantilever plate. The material model is assumed to be linear elastic and the material properties are given in Table 4. The overall length, width, and thickness of the structure is taken to be  $1 \times 1 \times 0.05$  m. Each ANCF element in its lateral direction is divided into 3 subdomains with 3 integration points per subdomain in order to account for the localized geometry. The loading function at point P which is the tip of the free end shown in Fig. 9 is linearly dependent on time and reaches its maximum value of  $-50$  N at  $t = 1$  s. Figures 10 and 11 show the convergence of the classical FE mesh and ANCF mesh for the given geometry, respectively, and Fig. 12 shows the error in the ANCF results against the converged classical FE solution. There is a small difference in the converged solutions of classical FE method and ANCF. This difference can be attributed to the way how each method accounts for the localized geometry in a different manner, however when compared to the total deformation of the structure, the difference in the vertical displacement of the tip point P is approximately 2.79%. Furthermore, Table 5 compares the ANCF solution for the same cantilever plate problem with and without the localized geometry details against a converged classical FE solution. Table 5 gives the vertical position of the tip point P shown in Fig. 9 at  $t = 1$  s. Accounting for the localized geometry has a softening effect on the structure since removing material in the longitudinal and lateral directions of the structure will reduce its

bending stiffness as can be seen from the ANCF and classical FE solutions with and without the local geometry. Thus the method proposed in this paper can successfully capture the effect of the localized geometry in a given ANCF mesh.

### 7.3 Tire Tread Contact Example

In this numerical example, a tire meshed with 240 ANCF plate elements is dropped on ground and the resulting contact patch is examined. NURBS is used to create the tire tread details, which are the grooves in the tire. This type of detail in the tire surface geometry is known as the rib type tread as shown in Table 1. The tire is based on the 45/65 R45 tire size and a nearly incompressible hyperelastic Mooney-Rivlin material is used to represent the rubber in the tread. Figure 13 shows the overall shape and cross section of the tire without any tread details. The material and contact parameters used for this example can be found in Tables 6 and 7 respectively. The NURBS method using parameter mapping is used to superimpose the localized tread geometry on the outer surface of the tire. Figure 14(a) shows the control points and the shape of the NURBS curve used for representing the grooves in the tire, whereas the contact patch from the tire-ground contact is shown in Fig. 14(b). Figure 14(b) clearly shows that the contact force is zero in the groove regions of the tire and the tire is supported on the rib regions that are in contact with the ground. Figure 15 shows the determinant of the Jacobian (matrix of position vector gradients) at the center point of the tire tread lower surface, clearly illustrating that the material stays nearly incompressible during the large deformation of the tire. This example clearly shows the effectiveness of the subdomain method in capturing the localized surface geometry in the case of tires in contact with ground using the ANCF framework.

Furthermore, in order to demonstrate the convergence of the model, the tire mesh is refined and the convergence of the model against results acquired from a commercial FE code is

shown in Fig. 16 through the evolution of the vertical position of node 1 on the tire mesh. The mesh code provided in Fig. 16 follows an  $n \times m$  format where  $n$  refers to the number of elements in the tire radial direction, whereas  $m$  refers to the number of elements in the tire lateral direction. The commercial FE code mesh consisted of 22,631 quadratic tetrahedral elements in order to be able to correctly capture the localized geometry on the surface of the tire. The material and contact parameters used for this convergence analysis are provided in Tables 6 and 7 respectively. For the ANCF results, selectively reduced integration was used on the volumetric term of the Mooney Rivlin material model, whereas full integration was used on the deviatoric terms. The small difference between the converged ANCF result and the commercial FE code results can be attributed to the presence of some shear locking in the model since the deviatoric term of the Mooney Rivlin model used full integration in the  $x$  and  $y$  element directions. The reason for this is the usage of subdomain integration in the element lateral direction which adds more integration points in that domain in order to capture the localized geometry. Reduced integration with subdomain integration would lead to 1 integration point in every subdomain which might lead to spurious modes, potential hourglassing in the elements and a very crude approximation of the localized geometry. The study of reduced integration with subdomain integration requires more investigation and will be considered as a topic of research in the future. These results also lead to the conclusion that special attention must be paid to the tire mesh discretization as well as element locking phenomena in order to have a good ANCF model that yields accurate results. Further validation is required to ensure the correlation with a physical model; however this study shows that the continuum-based fully parameterized plate element can achieve convergence with mesh refinement and locking alleviation techniques.

## 8. SUMMARY AND CONCLUSIONS

In this investigation, a method for the integration of localized surface geometry with fully parameterized ANCF elements is proposed. ANCF finite elements are used to create the global geometry and perform the FE/MBS analysis of the bodies. The surface geometry details can be added without refining the mesh to the scale of the detailed features. The localized surface may be represented by NURBS and can accurately describe complex geometric shapes such as a conic surface and freeform surface. The basic idea lies in the integration of the localized surface with the global surface by augmenting the geometry during the numerical integration process. Two methods for including the localized geometry in the ANCF elements are proposed. The overlapping method simply changes the thickness of the element using a function that is dependent on the lateral and longitudinal coordinates of the element. The domain trimming method takes advantage of the powerful NURBS geometry as a tool to trim the domain of original ANCF element according to the shape of the localized geometry. While using NURBS to define the localized geometry, a mapping between ANCF local coordinates and NURBS localized geometric parameters is used in both geometric integration methods. Furthermore, a comparison of two numerical integration methods, the global domain and the subdomain methods is presented in this investigation. The results show that the subdomain method is better suited for integrating complex geometry in ANCF elements since it has more flexibility in the distribution of the Gauss integration points. Using the subdomain method, any kind of geometry can be superimposed in the case of fully parameterized ANCF elements without the need for further mesh refinement during dynamic simulations. A cantilever plate example with localized surface geometry is provided to validate our method by comparing the simulation results obtained with the proposed methods against a commercial FE code. A model of a flexible ANCF



plate contacting with rigid ground is used to study the effect of the number of subdomains and the number of integration points per subdomain used in accounting for the localized geometry. Finally, a tire model meshed with ANCF plate elements and described by a hyperelastic incompressible Mooney-Rivlin material with four grooves integrated as localized surface geometry is considered. The results from the tire simulation that capture the effect of the grooves in the tire contact patch show the effectiveness of the proposed methods whereas the convergence study performed with the tire model helps support the basis of the proposed concepts by demonstrating that the model can achieve convergence with mesh refinement and reduced integration techniques which help alleviate locking.. In summary, the proposed method does a good job of capturing surface geometry without significantly increasing the computational cost that comes from mesh refinement. Future studies can be focused on eliminating the limitations of the method that include the fact that very localized deformations of the more intricate geometry cannot be easily captured since the element deformation field is still governed by its basis functions, and that the method will be challenging to use with very complex three dimensional changes in the structure's geometry. Studying the effects of reduced integration within the subdomain integration scheme can also be considered as a topic of future investigations.

### **ACKNOWLEDGMENT**

This work was supported, in part, by National Natural Science Foundation of China (No. 51375141), China Scholarship Council and the Fundamental Research Funds for the Central Universities (No. 2013B18214). This financial support is gratefully acknowledged.

## REFERENCES

1. ANSYS® Academic Research Mechanical APDL Documentation. ANSYS Inc. Release 15.0 (2013).
2. Bornemann, P. B., and Cirak, F., 2013, “A Subdivision-based Implementation of the Hierarchical B-spline Finite Element Method”, *Computer Methods in Applied Mechanics & Engineering*, Vol. 253, pp. 584–598.
3. Bouclier, R., Passieux, J. C., and Salaün, M., 2016, “Local Enrichment of NURBS Patches using a Non-intrusive Coupling Strategy: Geometric Details, Local Refinement, Inclusion, Fracture,” *Computer Methods in Applied Mechanics & Engineering*, Vol. 300, pp. 1–26.
4. Chemin, A., Elguedj, T., and Gravouil, A., 2015, “Isogeometric Local H-refinement Strategy Based on Multigrids,” *Finite Elements in Analysis & Design*, Vol. 100, pp. 77–90.
5. Cho, J. R., Kim, K. W., Yoo, W. S., and Hong, S. I., 2004, “Mesh Generation Considering Detailed Tread Blocks for Reliable 3D Tire Analysis”, *Advances in Engineering Software*, Vol. 35(2), pp. 105–113.
6. Das, M., Barut, A., and Madenci, E., 2010, “Analysis of Multibody Systems Experiencing Large Elastic Deformations”, *Multibody System Dynamics*, Vol. 23(1), pp. 1-31.
7. Forsey, D. R., and Bartels, R. H., 1998, “Hierarchical B-Spline Refinement”, *ACM SIGGRAPH Computer Graphics*, Vol. 22(4), pp.205-212.

8. Gantoi, F.M., Brown, M.A., and Shabana, A.A., 2013, "Finite Element Modeling of the Contact Geometry and Deformation in Biomechanics Applications", *ASME Journal of Computational and Nonlinear Dynamics*, Vol. 8 (4), doi: 041013-1 – 041013-11.
9. Gipser, M., 2005, "FTire: A Physically Based Application-Oriented Tyre Model for Use with Detailed MBS and Finite-Element Suspension Models", *Vehicle System Dynamics*, Vol. 43, pp. 76-91.
10. Ito, Y., Shih, A., Koomullil, R., Kasmai, N., Jankun-Kelly, M., and Thompson, D., 2009, "Solution Adaptive Mesh Generation using Feature-aligned Embedded Surface Meshes", *AIAA Journal*, Vol. 47(8), pp. 1879–1888.
11. Kagan, P., Fischer, A., and Bar-Yoseph, P. Z., 2003, "Mechanically Based Models: Adaptive Refinement for B-spline Finite Element", *International Journal for Numerical Methods in Engineering*, Vol. 57(8), pp. 1145–1175.
12. Kleiss, S. K., Juttler, B., and Zulehner, W., 2012, "Enhancing Isogeometric Analysis by a Finite Element-based Local Refinement Strategy", *Computer Methods in Applied Mechanics & Engineering*, Vol. 213-216, pp. 168–182.
13. Lan, P., and Shabana, A. A., 2010, "Integration of B-spline Geometry and ANCF Finite Element Analysis", *Nonlinear Dynamics*, Vol. 61(1-2), pp. 193–206.
14. Li, J., and Ke, Y., 2000, "Feature-based Surface Modeling of Complex Surface in Reverse Engineering", *Chinese Journal of Mechanical Engineering*, Vol. 36(5), pp. 18–22.
15. Lugner, P., Pacejka, H., and Plochl, M., 2005, "Recent Advances in Tyre Models and Testing Procedures", *Vehicle System Dynamics*, Vol. 43, pp. 413-436.

16. Mikkola, A. M. and Shabana, A. A., 2003, “A Non-incremental Finite Element Procedure for the Analysis of Large Deformation of Plates and Shells in Mechanical System Applications,” *Multibody System Dynamics*, Vol. 9(3), pp. 283–309.
17. Neto, M. A., Ambrosio, J. A. C., and Leal, R. P., 2004, “Flexible Multibody Systems Models using Composite Materials Components”, *Multibody System Dynamics*, Vol. 12(4), pp. 385–405.
18. Nicolas, G., and Fouquet, T., 2013, “Adaptive Mesh Refinement for Conformal Hexahedral Meshes,” *Finite Elements in Analysis & Design*, Vol. 67, pp. 1–12.
19. Ogden, R.W., 1984, *Nonlinear Elastic Deformations*, Dover Publications.
20. Orzechowski G., Frączek J., 2012, “ Integration of the Equations of Motion of Multibody Systems using Absolute Nodal Coordinate Formulation”, *Acta Mechanica et Automatica*, Vol. 6, pp. 75-83.
21. Orzechowski, G., and Fraczek, J., 2015, “Nearly Incompressible Nonlinear Material Models in the Large Deformation Analysis of Beams using ANCF”, *Nonlinear Dynamics*, Vol. 82, pp. 451-464.
22. Pacejka, H. B., 2006, *Tire and Vehicle Dynamics*, 3<sup>rd</sup> Edition, Society of Automotive Engineers (SAE), Warrendale, PA.
23. Patel, M., Orzechowski, G., Tian, Q., and Shabana, A. A., 2015, “A New Multibody System Approach for Tire Modeling using ANCF Finite Elements,” *Proceedings of Institute of Mechanical Engineers Part K: Journal of Multi-body Dynamics*, Vol. 230(1), pp. 69–84.
24. Piegl, L., Tiller, W., 1997, *The NURBS Book*, 2<sup>nd</sup> Edition, Springer-Verlag, Berlin Heidelberg.

25. Recuero, A.M., Aceituno, J.F., Escalona, J.L., and Shabana, A.A., 2014, “A Nonlinear Approach for Modeling Rail Flexibility Using ANCF Finite Elements”, *Nonlinear Dynamics*, Vol. 83(1), 463-481.
26. Sanborn, G. G., and Shabana, A. A., 2009, “A Rational Finite Element Method Based on the Absolute Nodal Coordinate Formulation”, *Nonlinear Dynamics*, Vol. 58(3), pp. 565–572.
27. Schillinger, D., Dedè, L., Scott, M. A., Evans, J. A., Borden, M. J., Rank, E., and Hughes, T. J. R., 2012, “An Isogeometric Design-Through-Analysis Methodology Based on Adaptive Hierarchical Refinement of NURBS, Immersed Boundary Methods, and T-spline CAD Surfaces,” *Computer Methods in Applied Mechanics & Engineering*, Vol. 249-252, pp. 116–150.
28. Schmidt, R., Wuchner, R., and Bletzinger, K.-U., 2012, “Isogeometric Analysis of Trimméd NURBS Geometries”, *Computer Methods in Applied Mechanics & Engineering*, Vol. 241-244, pp. 93–111.
29. Shabana, A. A., 1997, “Flexible Multibody Dynamics: Review of Past and Recent Developments”, *Multibody System Dynamics*, Vol. 1, pp. 189-222.
30. Shabana, A. A., and Yakoub, R.Y., 2001, “Three Dimension Absolute Nodal Coordinate Formulation for Beam Elements: Theory”, *ASME Journal of Mechanical Design*, Vol. 123, pp. 606-613.
31. Shabana, A. A., 2012, *Computational Continuum Mechanics*, 2<sup>nd</sup> Edition, Cambridge University Press, Cambridge.
32. Shabana, A. A., 2013, *Dynamics of Multibody Systems*, Fourth Edition, Cambridge University Press, Cambridge, England.

33. Shabana, A. A., 2014, “ANCF Reference Node for Multibody System Applications”, *IMechE Journal of Multibody Dynamics* (in press).
34. Shabana, A. A., 2015, “ANCF Tire Assembly Model for Multibody System Applications”, *ASME Journal of Computational and Nonlinear Dynamics*, Vol. 10(2), pp. 024504-1 – 024504-4.
35. Tian, Q., Chen, L. P., Zhang, Y. Q., and Yang, J. Z., 2009, “An Efficient Hybrid Method for Multibody Dynamics Simulation Based on Absolute Nodal Coordinate Formulation”, *ASME Journal of Computational and Nonlinear Dynamics*, Vol. 4, pp. 021009-1 - 021009-14.
36. Uhm, T.-K., and Youn, S.-K., 2009, “T-spline Finite Element Method for the Analysis of Shell Structures”, *International Journal for Numerical Methods in Engineering*, Vol. 80(4), pp. 507–536.
37. Wang, P., Xu, J., Deng, J., and Chen, F., 2011, “Adaptive Isogeometric Analysis using Rational PHT-splines”, *Computer Aided Design*, Vol. 43(11), pp. 1438–1448.
38. Wang, W., 2000, “Special Quadratic Quadrilateral Finite Elements for Local Refinement with Irregular Nodes,” *Computer Methods in Applied Mechanics & Engineering*, Vol. 182, pp. 109–134.
39. Yu, Z., Liu, Y., Tinsley, B., and Shabana, A. A., 2016, “Integration of Geometry and Analysis for Vehicle System Applications: Continuum-based Leaf Spring and Tire Assembly,” *ASME Journal of Computational and Nonlinear Dynamics*, Vol. 11, doi: 031011- 031011-11.

Table 1: Tread classification for commercial tires [<https://www.yokohamaotr.com/otr/tires-101/otr-technology/tread-designs>]






<i>Type</i>	<i>Pattern</i>	<i>Properties</i>
<b>Rock</b>		<ul style="list-style-type: none"> <li>• Application: Off-the-road vehicles (OTR)</li> <li>• Excellent cut resistance</li> <li>• Large ground contact area</li> </ul>
<b>Traction</b>		<ul style="list-style-type: none"> <li>• Application: High traction vehicle (OTR, truck)</li> <li>• Directional tread pattern</li> <li>• Excellent traction</li> </ul>
<b>Block/Lug</b>		<ul style="list-style-type: none"> <li>• Application: Trucks, OTR vehicles</li> <li>• Wide tread and rounded shoulders</li> <li>• Low contact pressure</li> <li>• Good on soft and muddy terrains</li> <li>• Excellent traction</li> </ul>
<b>Rib</b>		<ul style="list-style-type: none"> <li>• Application: Automotive, trucks</li> <li>• Grooves running parallel to direction of motion</li> <li>• High directional stability</li> <li>• Excellent fuel economy</li> </ul>
<b>Smooth</b>		<ul style="list-style-type: none"> <li>• Application: Underground mines, construction</li> <li>• High wear and cut resistance</li> <li>• Used for compaction and leveling</li> <li>• Narrow groove on edge used to measure tread wear</li> </ul>

Table 2: Material properties used in the plate contact example

<b>Linear Elastic</b>	
Density (kg/m <sup>3</sup> )	7860
Modulus of Elasticity (MPa)	0.2
Modulus of Rigidity (MPa)	0.1

Table 3: Contact parameters used in the plate contact example

<b>Parameter</b>	<b>Value</b>
Ground Stiffness (N/m)	8500
Ground Damping (N·s/m)	20.0
Friction Coefficient $\mu$	0.75

Table 4: Material properties used in the cantilever plate example

<b>Linear Elastic</b>	
Density (kg/m <sup>3</sup> )	2000
Modulus of Elasticity (MPa)	2.0
Modulus of Rigidity (MPa)	1.0

Table 5: Comparison of the cantilever plate tip vertical position with and without localized geometry

<b>Mesh</b>		<b>With Local Geometry (m)</b>	<b>Without Local Geometry (m)</b>
ANCF	2×2	-0.4098	-0.3763
	3×3	-0.4649	-0.4332
	4×4	-0.5030	-0.4654
	5×5	-0.5232	-0.4774
	6×6	-0.5335	-0.4853
	8×8	-0.5412	-0.4928
	12×12	-0.5469	-0.4966
	16×16	-0.5511	-0.4981
Classical FE converged mesh		-0.5669	-0.5022

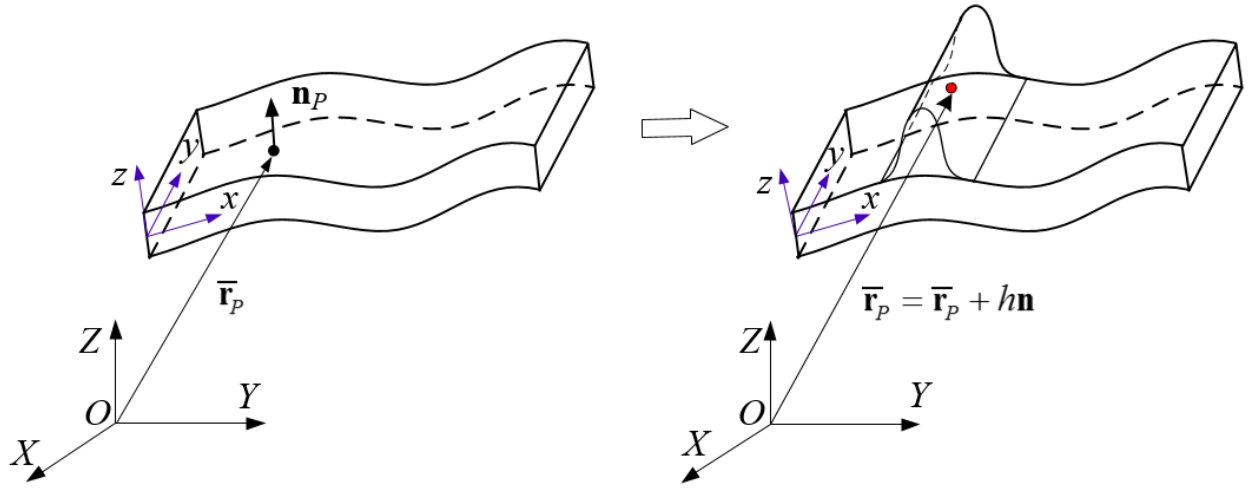


Table 6: Material properties used in the tire example

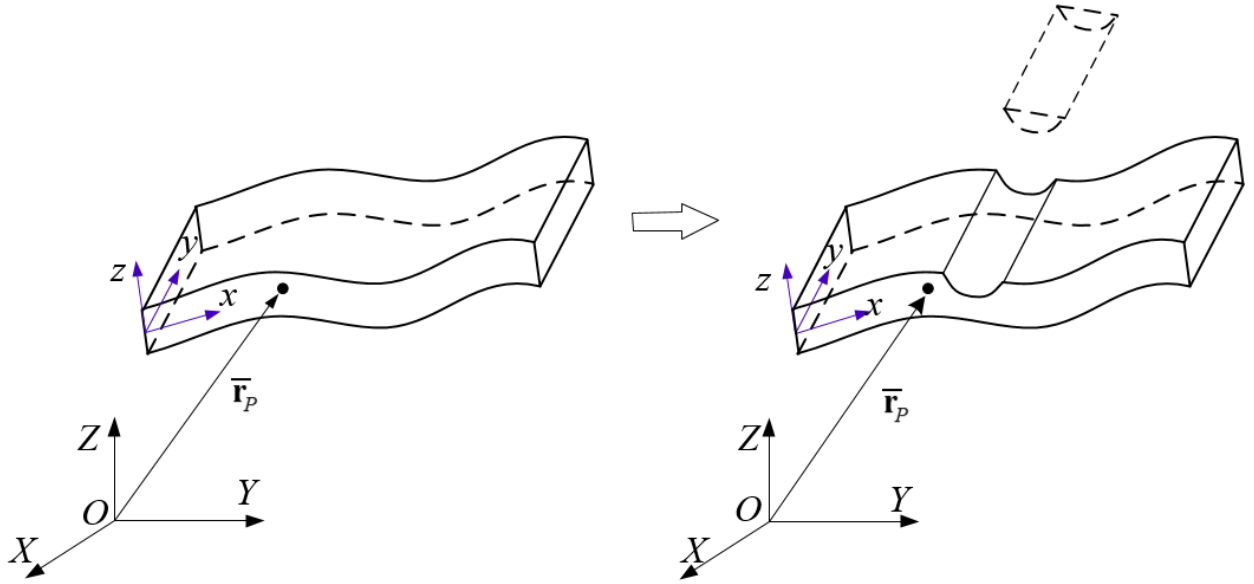
<b>Mooney-Rivlin</b>	
Density ( $\text{kg/m}^3$ )	1500
Coefficient $\mu_{10}$ (MPa)	2.5
Coefficient $\mu_{01}$ (MPa)	2.0
Penalty coefficient $k$	$1.33 \times 10^8$

Table 7: Contact parameters used in the tire example

<b>Parameter</b>	<b>Value</b>
Ground Stiffness (kN/m)	70
Ground Damping (N·s/m)	160
Friction Coefficient $\mu$	0.75



(a) Overlapping method



(b) Domain trimming method

Figure 1. Integration of localized geometry with ANCF geometry

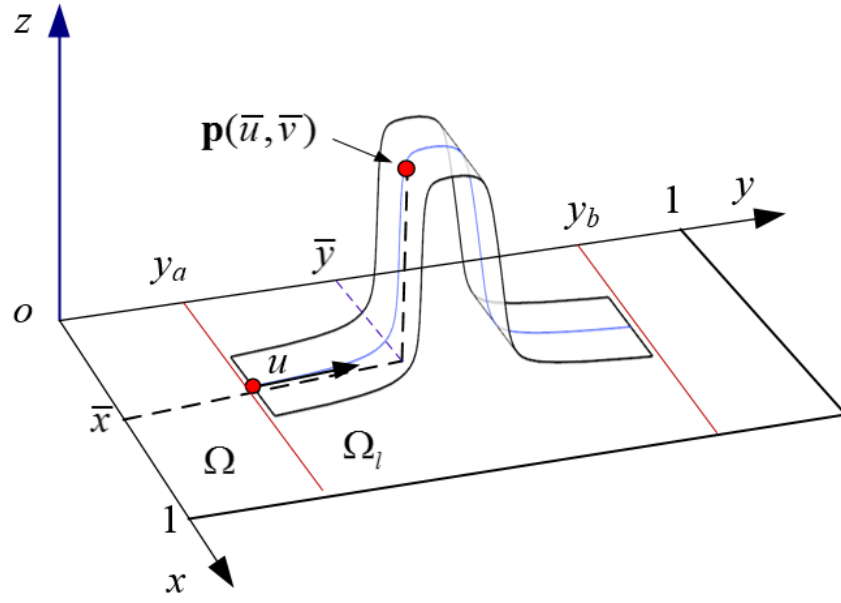
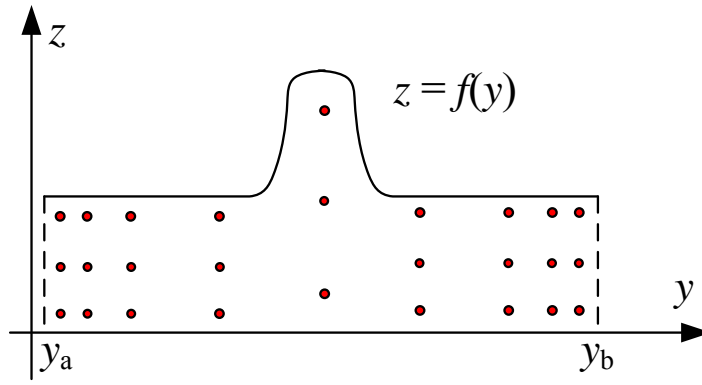
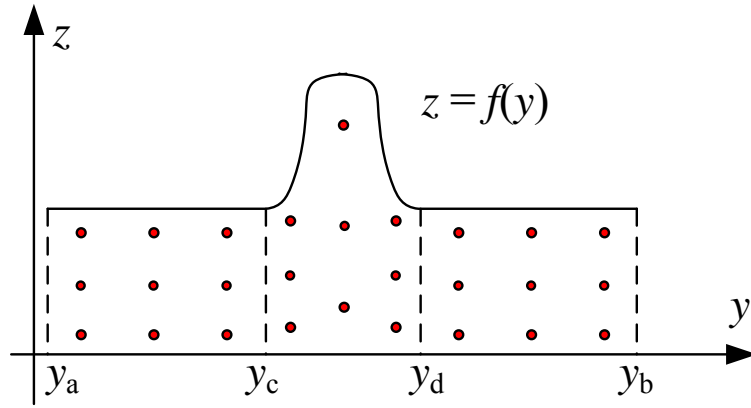


Figure 2. Mapping between the localized geometry parameters and ANCF element coordinates

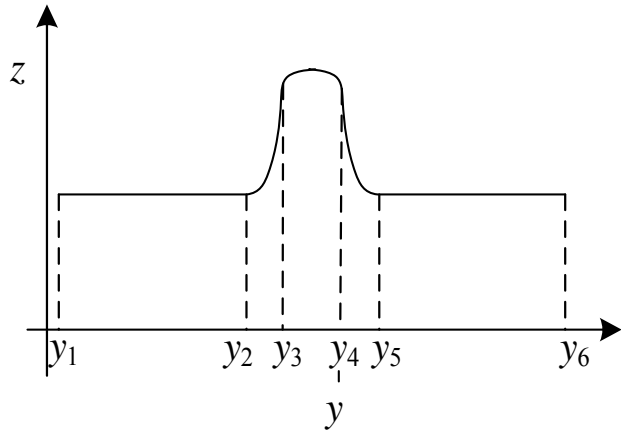


(a) Global domain method

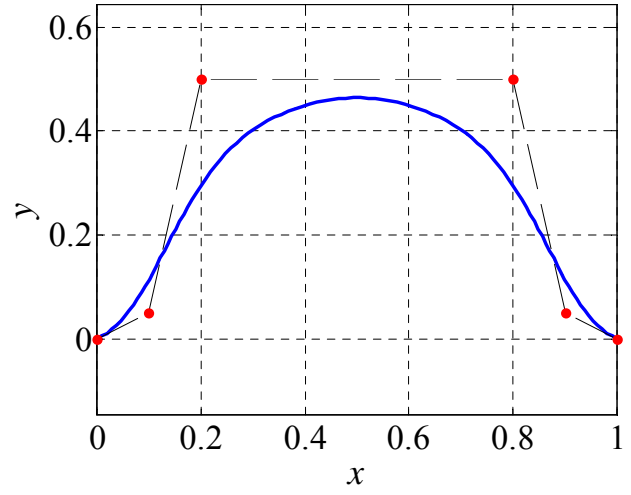


(b) Subdomain method

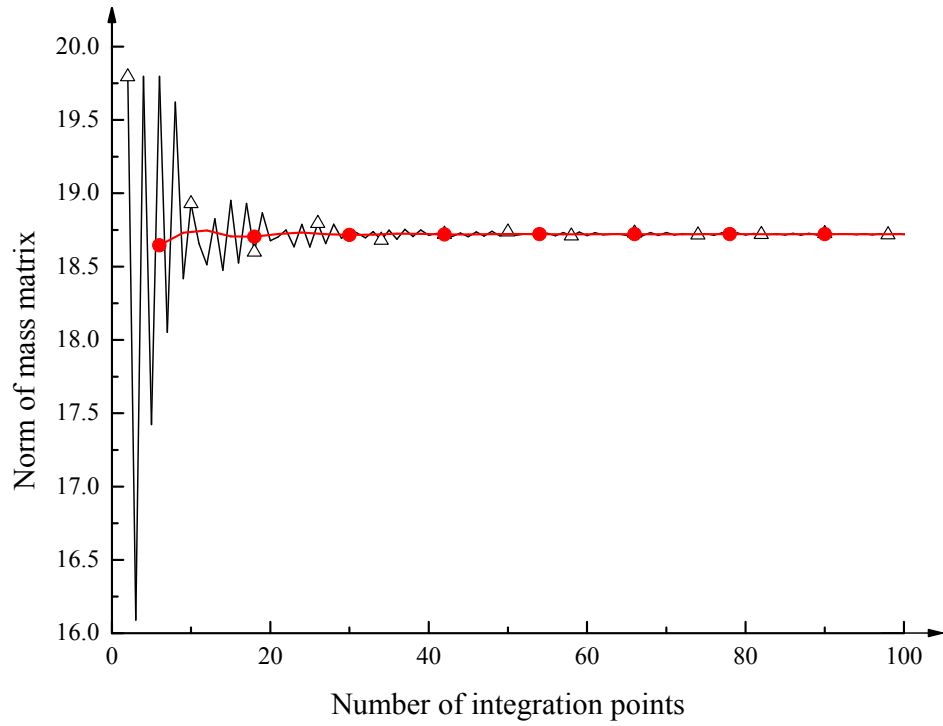
Figure 3. Distribution of integration points using the global domain and subdomain methods



(a) Division of subdomain

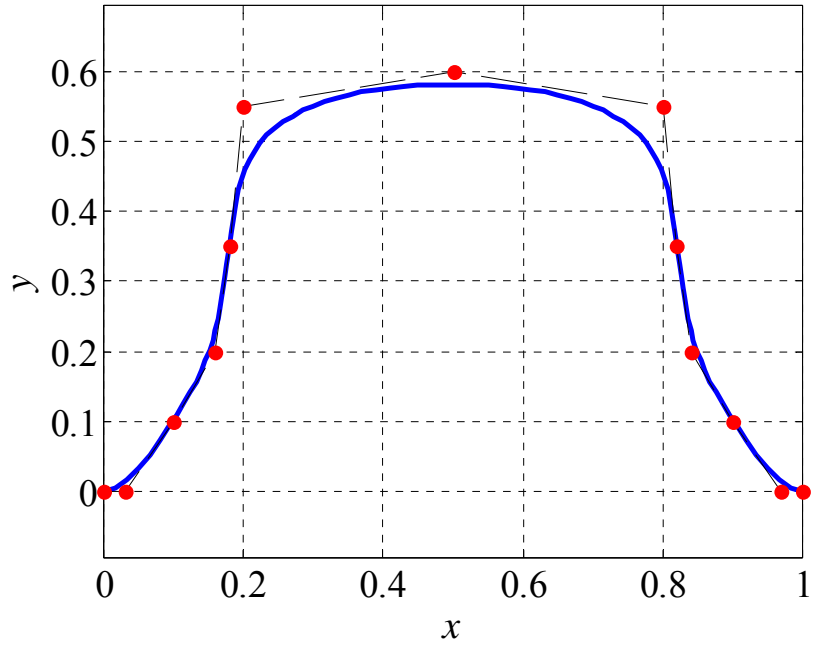


(b) Localized geometry  
( ● Control point)

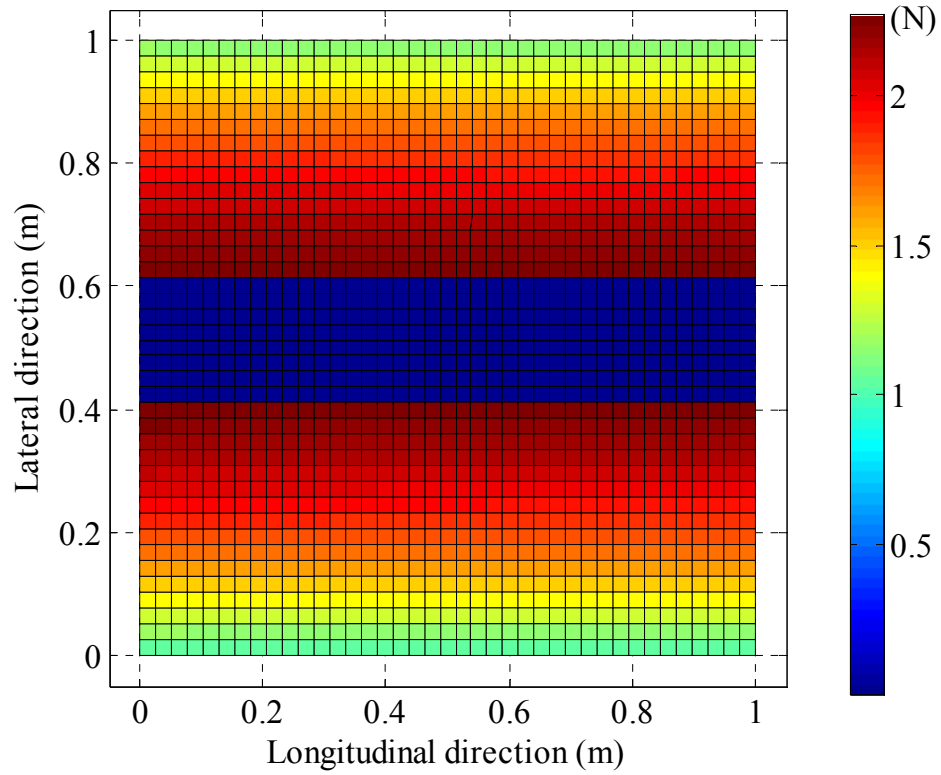


(c) Comparison of mass matrix norm using the two integration methods  
( —△— Global domain —●— Subdomain )

Figure 4. Comparison of global domain and subdomain integration method



(a) The definition of localized geometry  
( ● Control point)



(b) Contact force at  $t=1.0s$

Figure 5. One-plate contact example

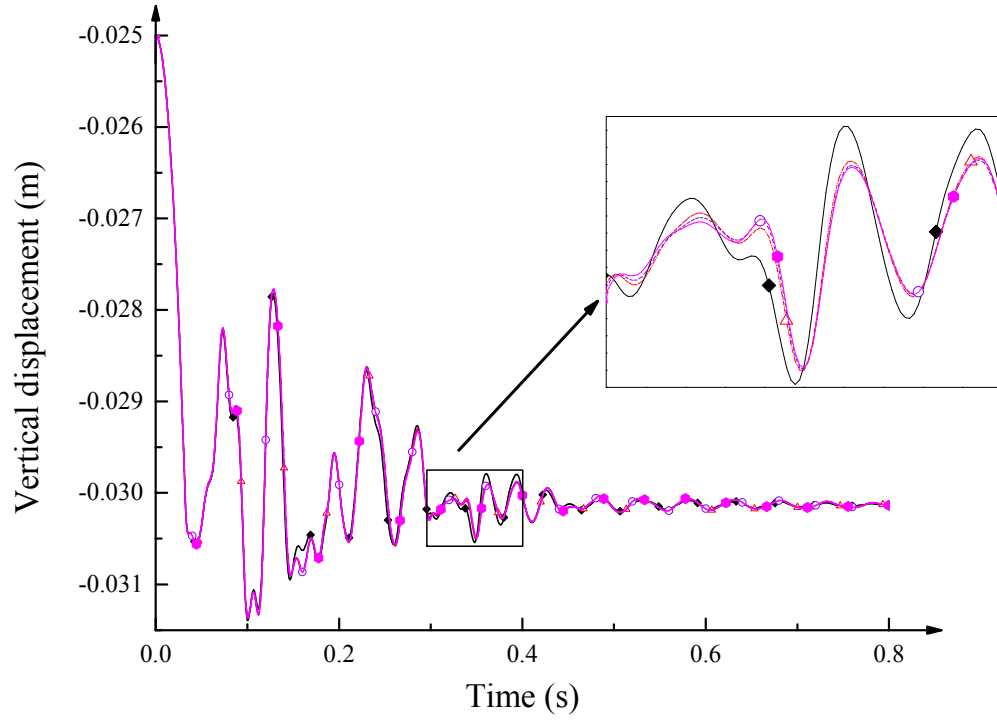


Figure 6. Vertical displacement using different numbers of integration points  
 ( —◆— 2 points    - -△- - 3 points    - -○- - 4 points    —●— 5 points )

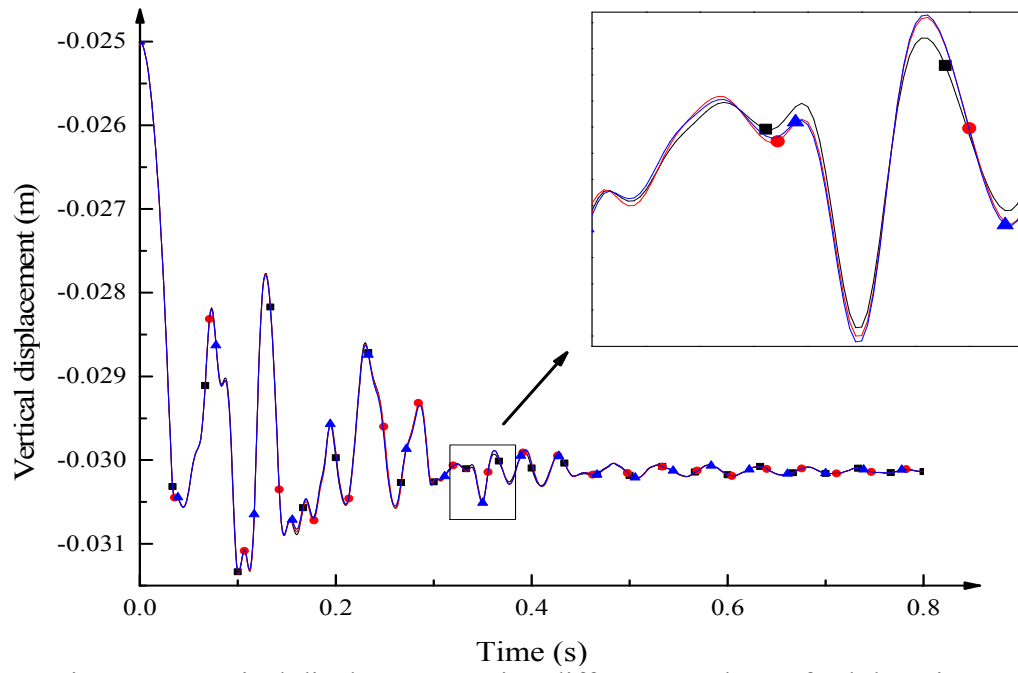
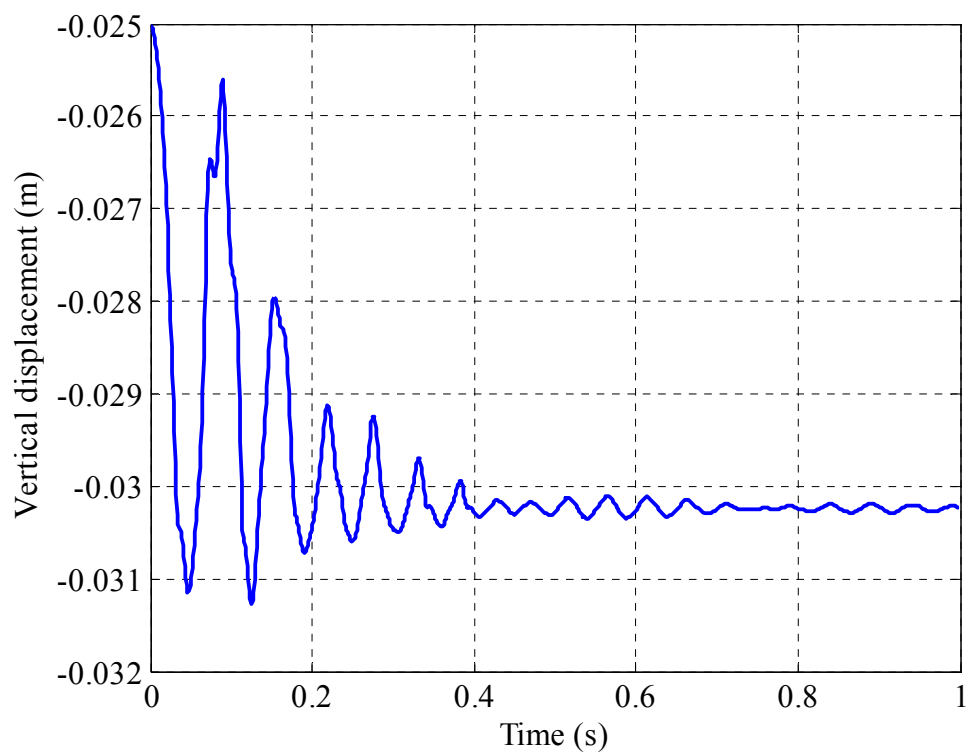
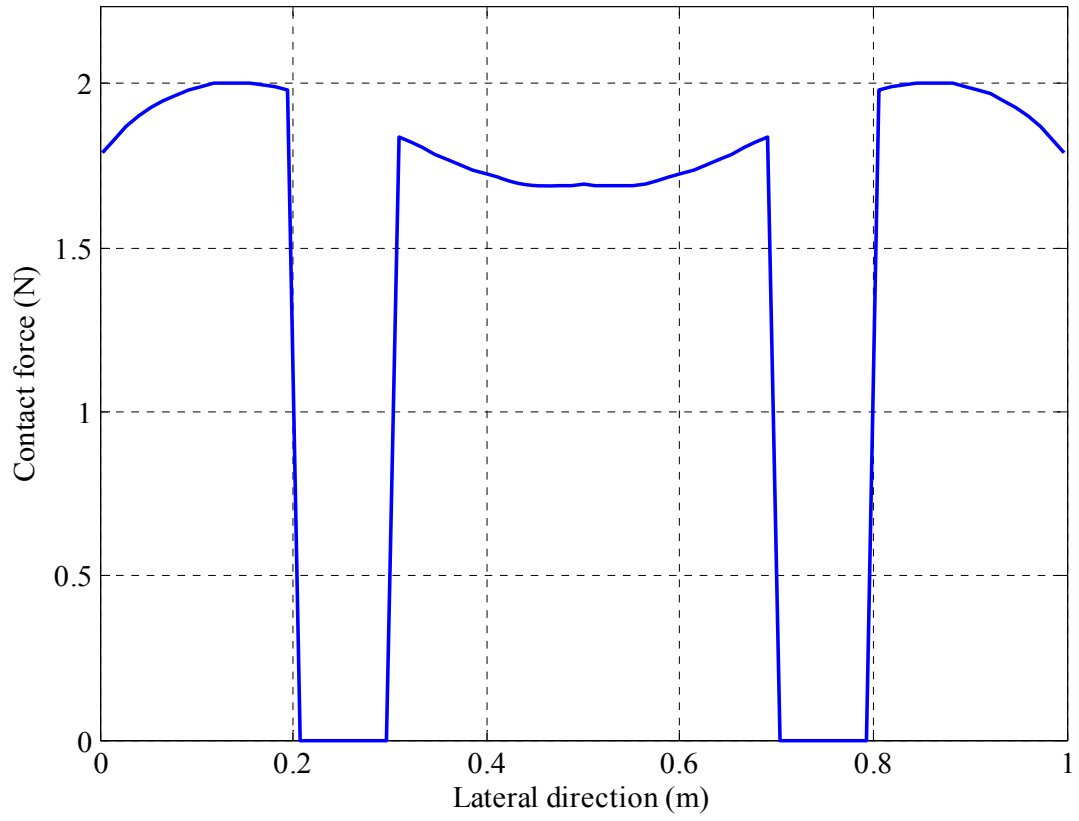


Figure 7. Vertical displacement using different numbers of subdomains  
 ( —■— 2 subdomains    —●— 3 subdomains    —▲— 4 subdomains )

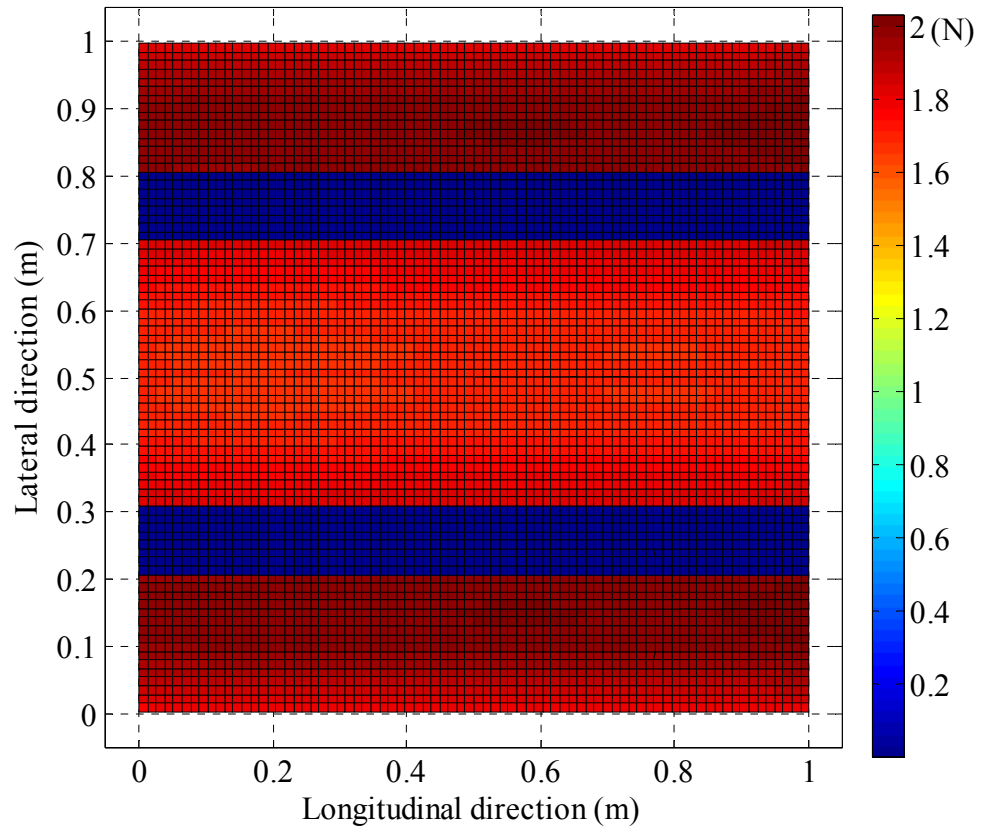


(a) Vertical displacement of contact point





(b) Contact force distribution at the structure mid-section at  $t = 1.0$  s



(c) Contact force at  $t = 1.0\text{s}$

Figure 8.  $2 \times 2$  ANCF plate element mesh with localized geometry

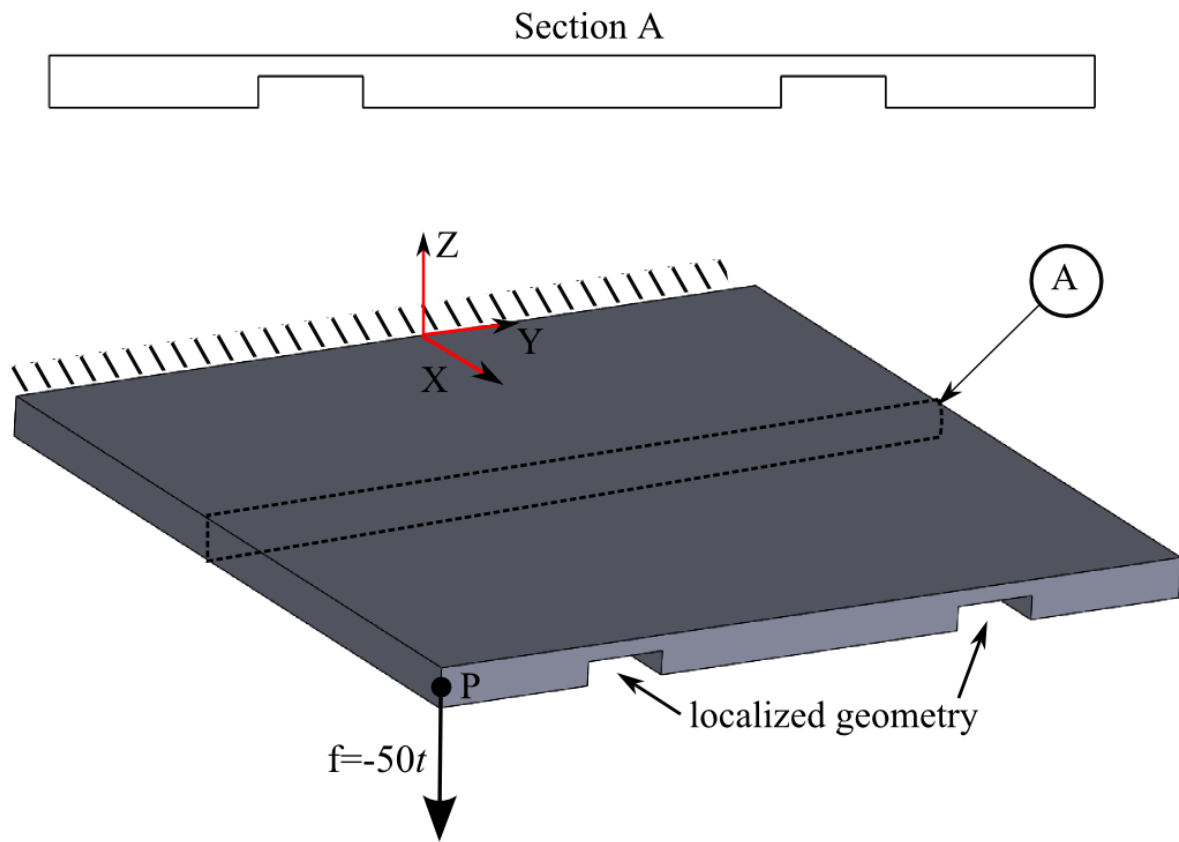


Figure 9. Cantilever plate reference configuration and cross section

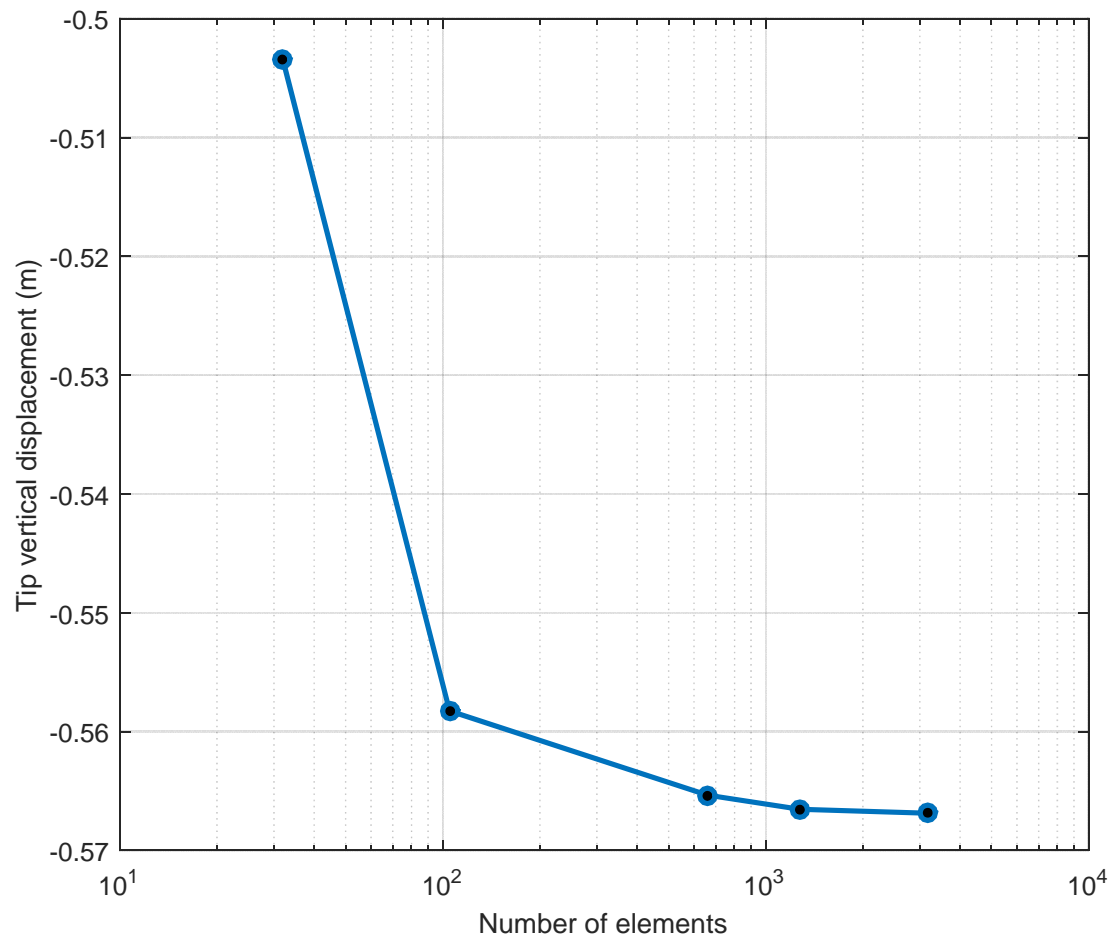


Figure 10. Convergence of classical FE code solution for plate structure with local geometry

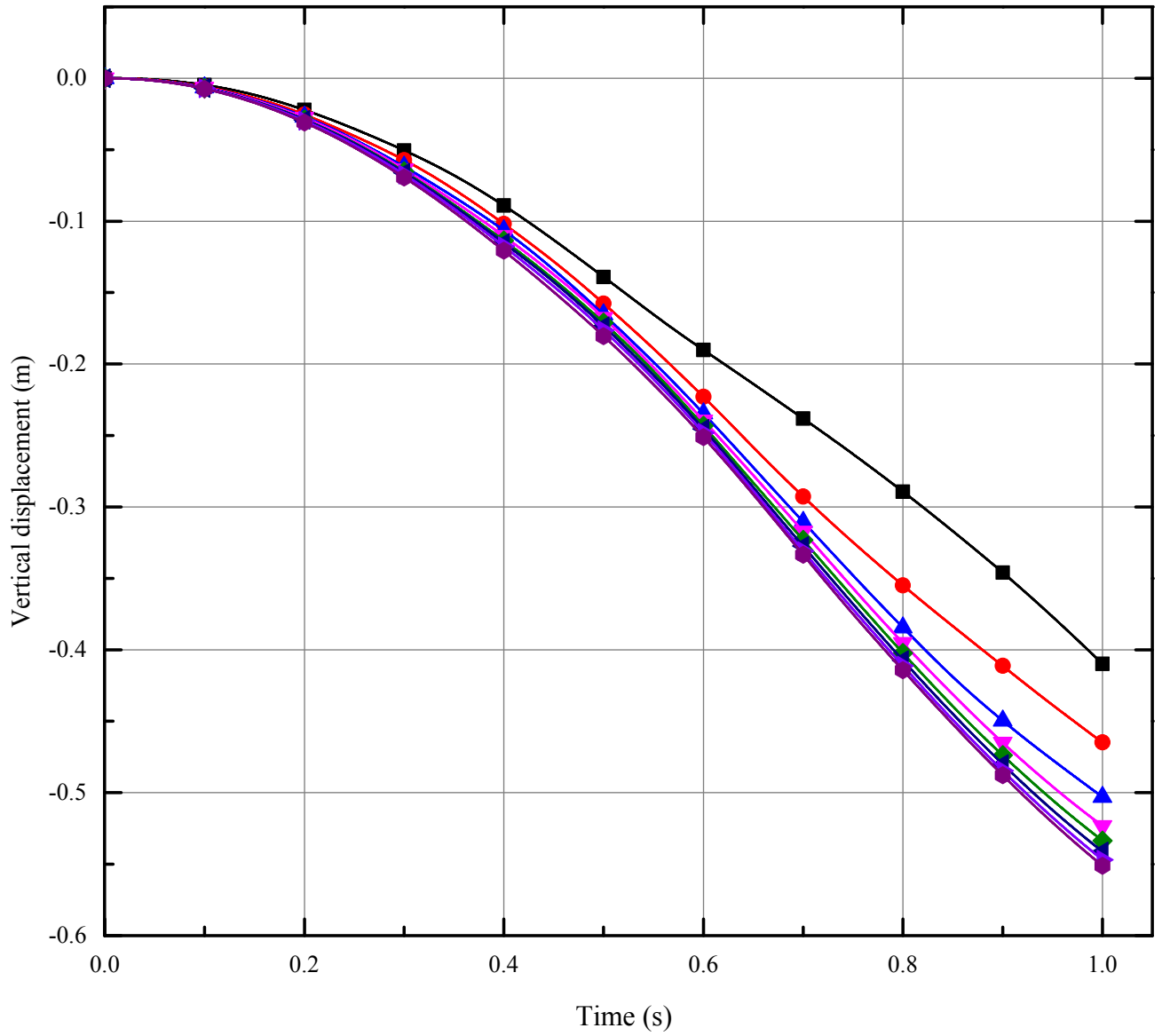


Figure 11. Convergence of ANCF solution for plate structure with local geometry

( —■— 2X2 —●— 3X3 —▲— 4X4 —▼— 5X5 —◆— 6X6 —◀— 8X8 —▶— 12X12 —●— 16X16 )

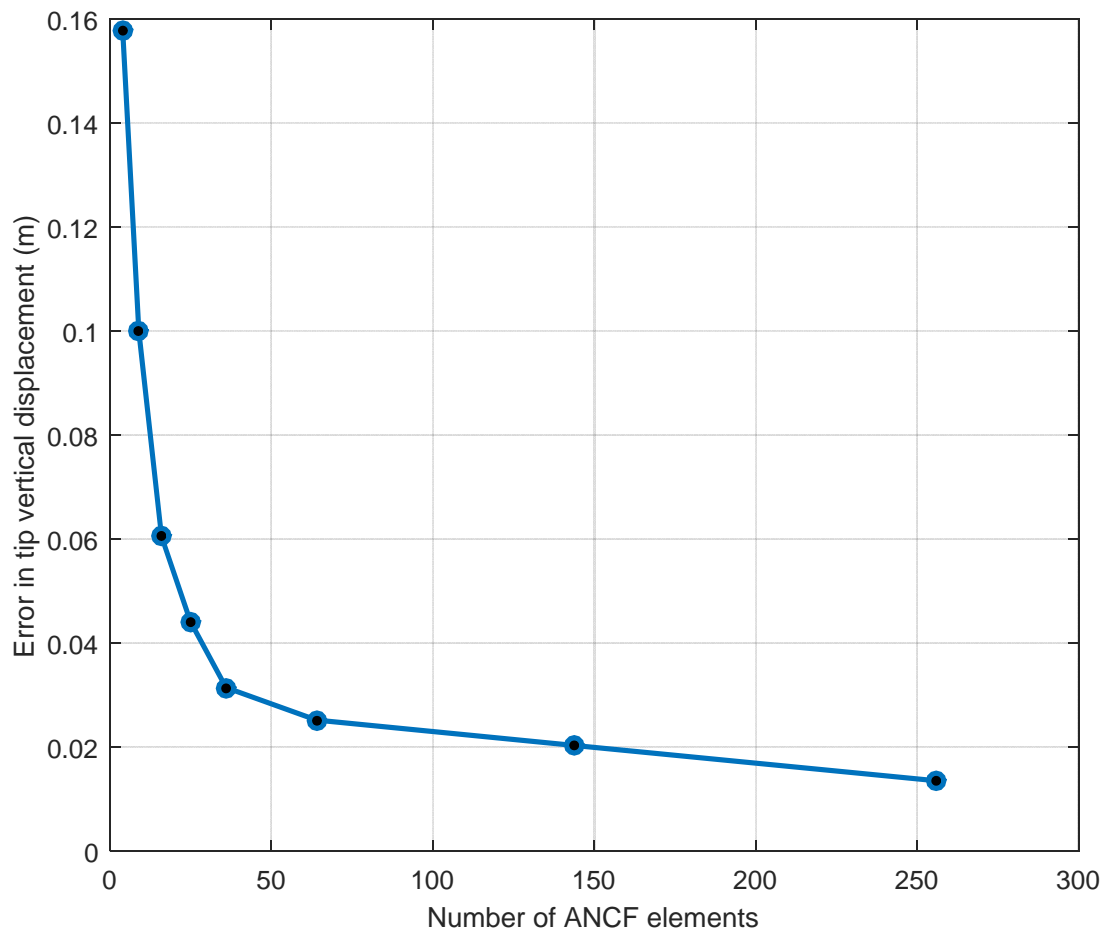


Figure 12. Difference between ANCF solution and classical FE solution

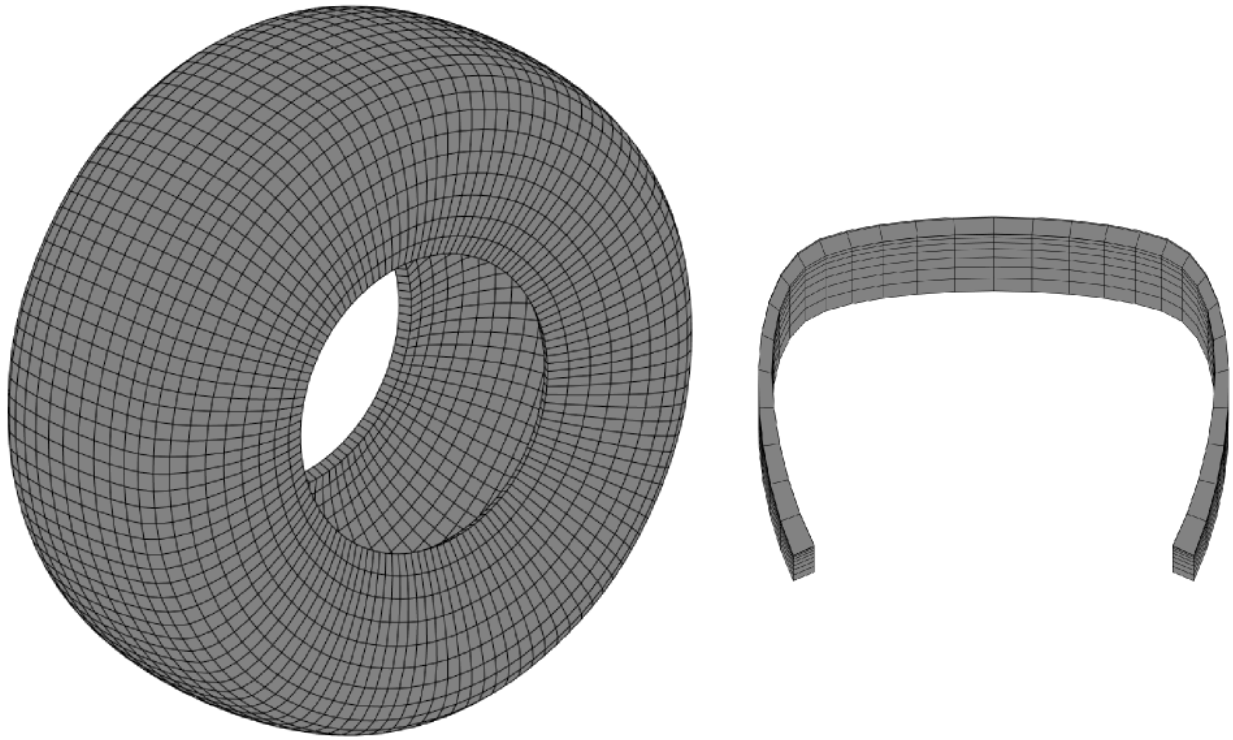
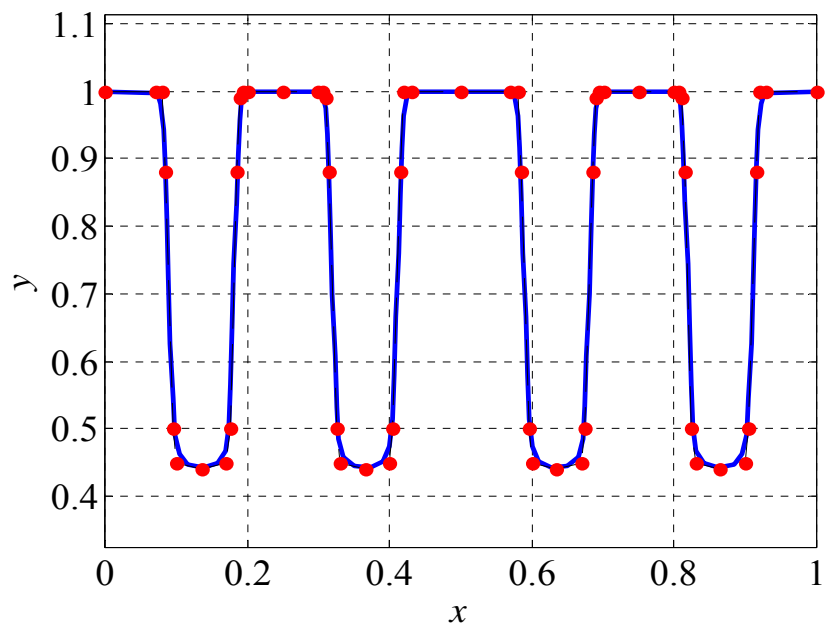
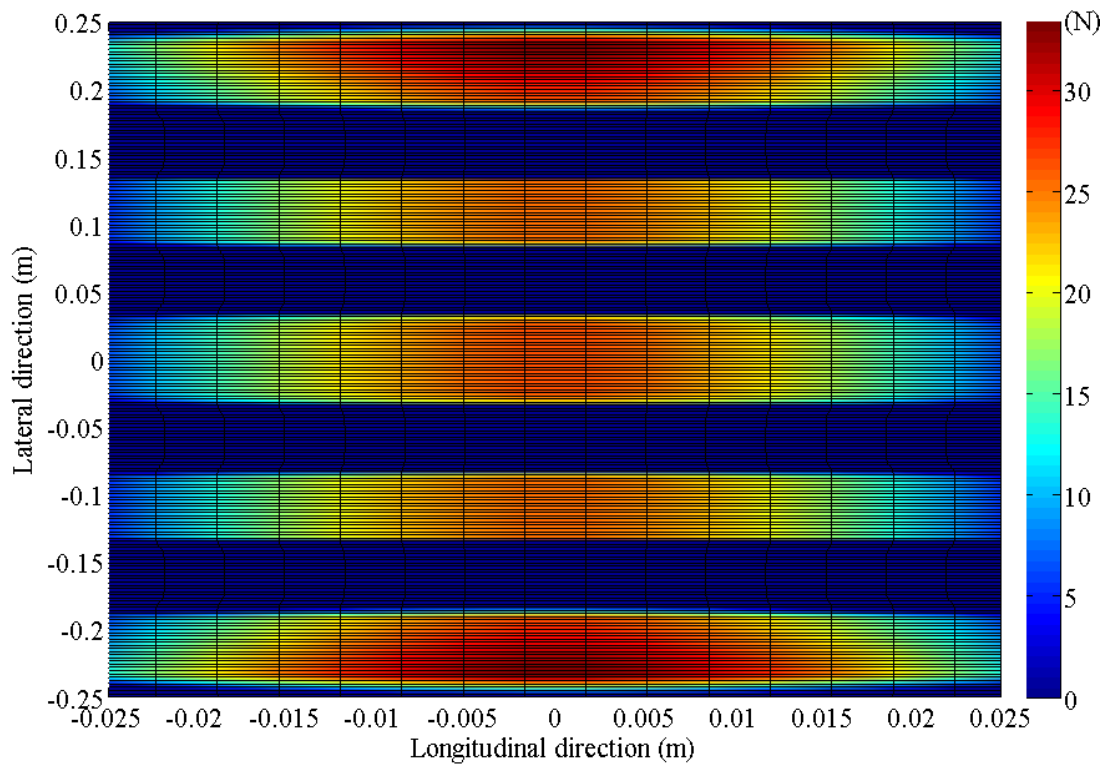


Figure 13. ANCF tire geometry and tread shape



(a) Localized surface geometry of the tire tread  
(● Control point)



(b) Tire tread contact patch  
Figure 14. Tire tread with four grooves



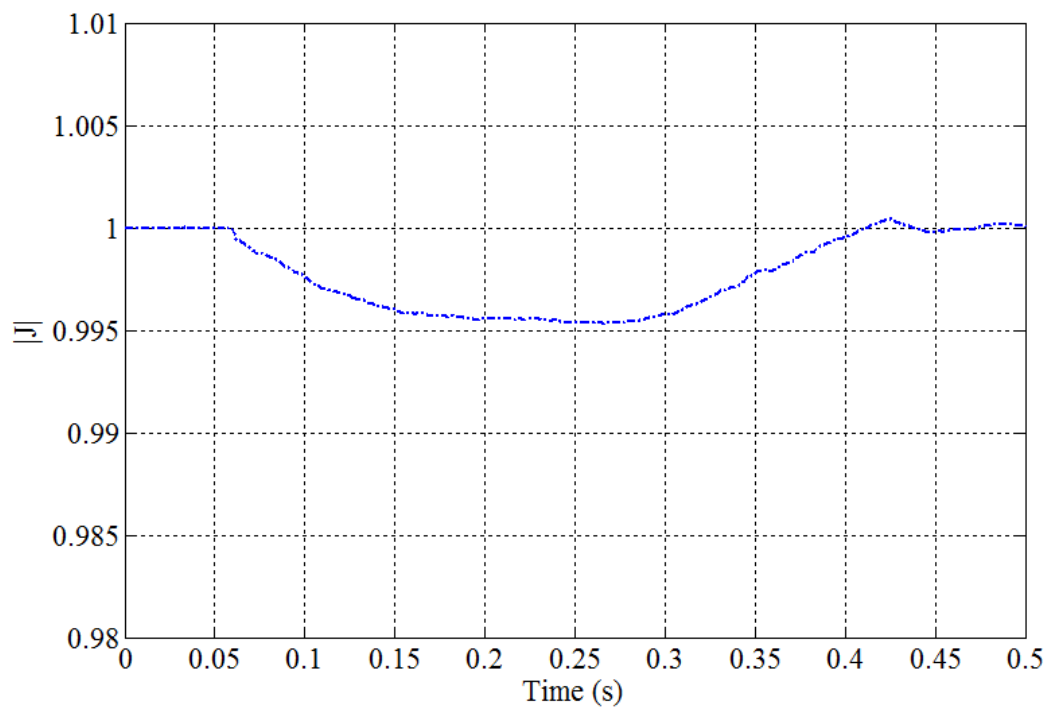


Figure 15. Value of  $|J|$  at the middle point on the bottom of the tire tread surface

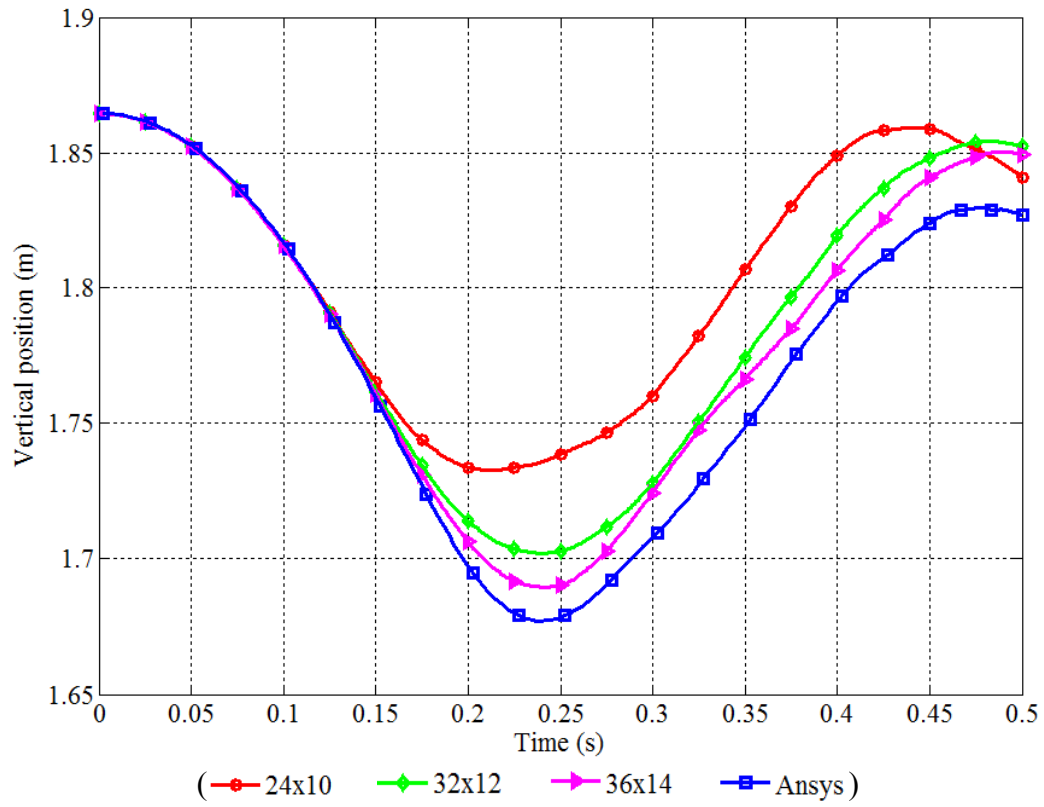


Figure 16. Position convergence of ANCF solution for tire contact example